JACS
JOURNAL OF THE AMERICAN CHEMICAL SOCIETY

Article

pubs.acs.org/JACS

Enclathration and Confinement of Small Gases by the Intrinsically 0D Porous Molecular Solid, Me,H,SiMe$_2$

Christopher M. Kane,[†] Arash Banisafar,[†] Timothy P. Dougherty,[†] Leonard J. Barbour,[‡] and K. Travis Holman*[,†]

[†]Department of Chemistry, Georgetown University, 37th and O Streets NW, Washington, D.C. 20057, United States

[‡]Department of Chemistry, University of Stellenbosch, 7602, Stellenbosch, South Africa

Supporting Information

ABSTRACT: The stable, guest-free crystal form of the simple molecular cavitand, **Me,H,SiMe$_2$**, is shown to be intrinsically porous, possessing discrete, zero-dimensional (0D) pores/microcavities of about 28 Å^3. The incollapsible 0D pores of **Me,H,SiMe$_2$** have been exploited for the enclathration and room temperature (and higher) confinement of a wide range of small gases. Over 20 isostructural x(gas/guest)@**Me,H,SiMe$_2$** ($x \leq 1$) clathrates (guest = H_2O, N_2, Ar, CH_4, Kr, Xe, C_2H_4, C_2H_6, CH_3F, CO_2, H_2S, CH_3Cl, CH_3OCH_3, CH_3Br, CH_3SH, CH_3CH_2Cl, CH_2Cl_2, CH_3I, CH_3OH, $BrCH_2Cl$, CH_3CH_2OH, CH_3CN, CH_3NO_2, I_2), and a propyne clathrate (CH_3CCH@**Me,H,SiMe$_2$**·2$CHCl_3$), have been prepared and characterized, and their single crystal structures determined. Gas enclathration is found to be highly selective for gases that can be accommodated by the predefined, though slightly flexible 0D pore. The structure determinations provide valuable insight, at subangstrom resolution, into the factors that govern inclusion selectivity, gas accommodation, and the kinetic stability of the clathrates, which has been probed by thermal gravimetric analysis. The activation (emptying) of several clathrates (guest = H_2O, N_2, CO_2, Kr, CH_3F) is shown to occur in a single-crystal-to-single-crystal (SC → SC) fashion, often requiring elevated temperatures. Akin to open pore materials, water vapor and CO_2 gas are shown to be taken up by single crystals of empty **Me,H,SiMe$_2$** at room temperature, but sorption rates are slow, occurring over weeks to months. Thus, **Me,H,SiMe$_2$** exhibits very low, but measurable, gas permeability, despite there being no obvious dynamic mechanism to facilitate gas uptake. The unusually slow exchange kinetics has allowed the rates of gas (water vapor and CO_2) sorption to be quantified by single crystal X-ray diffraction. The data are well fit to a simple three-dimensional diffusion model.

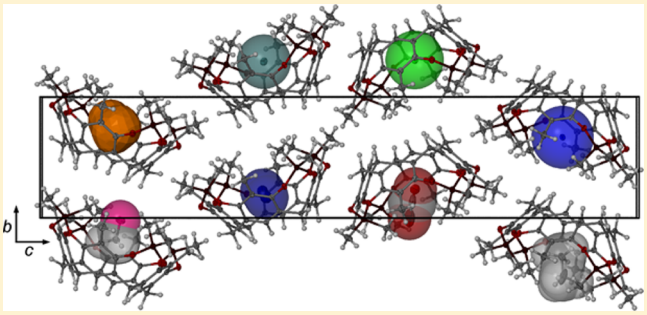

INTRODUCTION

There is much contemporary interest in the development of new microporous materials for applications of light gas complexation/capture, storage, and/or separations.[1] In the past 15 or so years, as the power of synthetic organic chemistry has been brought to bear on the synthesis of microporous materials, new classes of molecule-derived gas sorbents and storage materials have emerged, including coordination polymers and metal−organic frameworks (MOFs),[2] covalent organic frameworks (COFs),[3] and polymers of intrinsic microporosity (PIMs).[4] These materials are porous by design, wherein judicious polymeric connection (covalent, coordinate covalent) of shape-persistent molecular components sustains interconnected pores. Concomitant to the development of framework-type porous materials has been the (re)emergence of porous molecular solids.[5−7] Being composed of discrete molecules, porous molecular solids offer potential advantages over polymeric frameworks, including solubility (processing advantages), chemical/synthetic diversity, the ability to mix-and-match components (e.g., as cocrystals[8] or solid solutions), and the general mobility of molecular components that are relatively weakly connected. In this context, shape-persistent, effectively incollapsible macrocycles—e.g., cavitands[9] (Scheme 1), calix[n]arenes,[10,11] cryptophanes,[12] (hemi)carcerands,[13] cucubiturils,[14] metal−organic cages[15] or metallocycles,[16,17] and organic cages[5,18−20]—have been recognized as candidate porous molecular solids[6] and even as active ingredients in the emerging area of porous liquids.[21] Many of these compounds are intrinsically porous in the sense that, in pure (apohost) form, they are simply incapable of filling all of the potentially useful space in the solid. And while many of these compounds have long been recognized for their ability to bind small molecules, ions, and sometimes gases in solution, their materials properties are only recently being vetted in relation to gas capture.[9,10,12−14]

Porosity (ε) is defined by IUPAC as "the ratio of the total pore volume to the apparent volume of the particle."[22] The term "porous", however, does not imply the presence of connected pores, or even permeability of a porous solid. Importantly, IUPAC recognizes the difference between *open* porosity,

Received: October 30, 2015
Published: March 8, 2016

DOI: 10.1021/jacs.5b11395
J. Am. Chem. Soc. 2016, 138, 4377−4392

Scheme 1. Schematic Representation of Open Porosity (Left, 1D Pores) and Closed Porosity (Right, 0D Pores)[a]

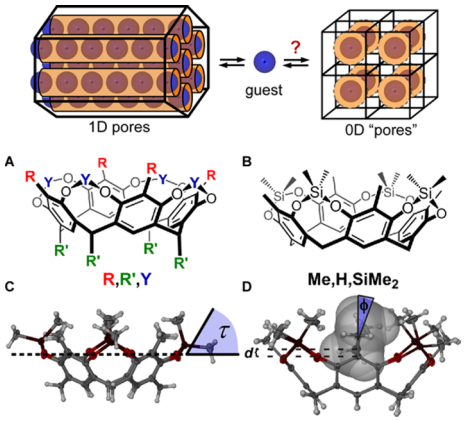

[a]The crystalline sorbate host matrices are transparent and are depicted to be fully loaded with a complementary gas sorbate (blue). The internal pore surfaces are colored orange. The question mark is meant to suggest that the time scales and mechanisms of gas exchange by 0D porous crystalline structures remain poorly understood. (A, B) Molecular structures of some 0D porous cavitands, identified by their rim (**R**), feet (**R′**), and bridging (**Y**) groups. All compounds are *rccc* stereoisomers, unless otherwise noted. (C) The angle between the plane defined by an O−Si−O linkage and the plane of the cavitand oxygen atoms (τ) quantifies the conformation of the dimethylsilyl groups in **Me,H,SiMe$_2$**. (D) The depth of penetration of a guest within the cavitand bowl, d (Å), defined by the distance between the most penetrating heavy atom and the plane of upper arene carbon atoms of the host. The angle between the long axis of a linear guest and the pseudo-C_4 axis of the cavitand, as illustrated for the $x(C_2H_6)$@**Me,H,SiMe$_2$** clathrate, is defined as ϕ.

referring to the pores accessible to a given probe molecule, and *closed* porosity, referring to zero-dimensional (0D) pores. The closed (0D) pores of such materials are broadly thought to be "inactive in such processes such as fluid flow and adsorption of gases"[22] (Scheme 1) and so are occasionally, though inaccurately, categorized as nonporous solids. Thus, while it may be reliably predicted that the crystalline structures of certain shape-persistent macrocycles ought to exhibit empty potentially useful space, such spaces need not be interconnected. Indeed, the solid forms of many macrocycles may instead exhibit 0D pores or micro*cavities*, wherein the windows between void spaces in the solid are less than the diameter of individual atoms, at least in the static view of their structures.

Certain container compounds exhibit 0D pores by virtue of their closed-window molecular structures. We have recently shown, for example, that empty crystal forms of (±)-cryptophane-111 and its derivatives are 0D porous materials.[12] Relatedly, open-window or open-ended macrocycles may pack in such a way that their intrinsic molecular cavities are empty, but isolated from one another, resulting in 0D porous structures. Some of us have shown, for example, that various calix[*n*]arenes[10] and, more recently, the structurally similar resorcin[4]arene-based cavitands[9] adopt intrinsically 0D porous structures in the solid state.

Historically, crystalline materials exhibiting occupied cavities are referred to as clathrates.[23] Importantly, however, relatively few clathrate-forming molecular compounds have been shown to sustain 0D porous structures in the absence of enclathrated guests.[24] And many of these, including the much studied *tert*-butylcalix[4]arene, are metastable structures that can collapse to give close-packed phases.[25−27] In fact, the structural demonstration of empty, molecule-sized (> ∼25 Å^3), 0D pores in molecular crystalline solids remains rare.[28−30] We have recently argued,[9] however, that the paucity of such structures is likely due to experimental biases related to: i) the fact that such compounds are predisposed to form solvates when crystallized from solution, (ii) that solvates tend to lose single crystallinity during solvent loss, giving powders and (iii) the relative challenges associated with structure determination of molecular materials by powder diffraction as compared to single crystal diffraction. We feel it likely, therefore, that 0D porous molecular solids are prevalent, though their structures have largely gone uncharacterized. For example, Dalcanale and co-workers have extensively studied the sorptive and sensory properties of various, almost certainly porous, cavitand materials, often without specific knowledge of the solid state structures.[31]

The question of whether a pore is active with respect to fluid flow greatly depends upon experimental conditions and, for 0D pores, is largely a question of mechanism, kinetics, and structural dynamics. Materials with seemingly closed (or collapsed) pores can exhibit unusual sorption/desorption properties, including temperature[32] or pressure-induced gating effects,[33,34] attributable to a structural change that opens or dilates pore windows. Other closed pore materials display so-called transient porosity, wherein conformational dynamics in the solid are thought to allow for temporary opening of windows through which sorbents may diffuse. *tert*-Butylcalix[4]arene,[11] certain metal−organic macrocycles,[17] and **CC-3** are examples of porous molecular solids that appear to exhibit this behavior.[18] At the opposite end of the pore accessibility/activity spectrum are molecular solids that kinetically trap volatile species in their 0D pores during clathrate formation.[29] Such materials may find niche applications in the longer term storage of gases, in the protection of reactive compounds,[35] as high temperature sorbents, *etc.* For example, the extrinsic microcavities of the empty form of calix[4]arene can be induced to trap Freons, methane, or other gases and hold them well above room temperature.[17] And we have recently shown that the intrinsic cavity of (±)-cryptophane-111 can confine xenon to unprecedented temperatures (∼300 °C).[12a] Still other 0D porous molecular solids—e.g., hydroquinone, C_{60} (interstices)—are known to form kinetically stable gas clathrates.[36] Indeed, the closed-pore to micropore structural regime warrants systematic exploration, particularly in the context of gas complexation, confinement/permeability, and separations.

It stands to reason that the kinetic confinement properties of 0D porous materials will be optimized in materials with small and *inflexible* pore apertures that limit the possibility of transient porosity offered by dynamic functional groups. Clathrasils[37] and blocked-pore zeolites[38] are exemplary inorganic materials that satisfy this condition and can kinetically trap gases at high temperatures, but their insoluble framework structures do not allow for easy assembly or disassembly of the pores. Porous molecular solids, on the other hand, are soluble and allow for simple mechanisms of guest capture (e.g., slurrying or crystallization under gas pressure) and release (e.g., by simple dissolution). Herein, we revisit one member of Cram's[39] family of molecular cavitands (**R,R′,Y**; Scheme 1), namely **Me,H,SiMe$_2$**,[40] as an intrinsically 0D porous molecular solid. The inflexibility of **Me,H,SiMe$_2$** is exploited for the selective capture and relatively high temperature confinement of small gases in the solid state. Characterization of over 20 different isostructural gas clathrates and solvates by single crystal diffraction provides a structural basis for understanding: (i) the selectivity of the

DOI: 10.1021/jacs.5b11395
J. Am. Chem. Soc. 2016, 138, 4377−4392

enclathration process and the relative affinity of the 0D porous **Me,H,SiMe$_2$** host matrix for the various guests, (ii) the stress and strain relationship between host and the encapsulated gases/solvents, and (iii) its consequences on the relative kinetic stabilities of the various clathrates. Also, despite there being no obvious dynamic mechanism to permit guest exchange, 0D porous crystals of **Me,H,SiMe$_2$** are shown to be permeable to certain gases (both desorption and sorption) without deterioration of their single crystallinity. As anticipated, the kinetics of gas sorption and desorption are found to be extremely slow at room temperature, and this feature is exploited in the measurement of water vapor and CO_2 sorption kinetics by single crystal X-ray diffraction. These analyses shed light on issues of gas binding and confinement, sorbent/sorbate dynamics, and structural flexibility at the sub-angstrom length scale, properties that cannot as easily be studied in large-pore materials.[17,41,42]

RESULTS AND DISCUSSION

1. Background and Hypothesis. We have recently demonstrated that, as expected, the most thermodynamically stable empty apohost crystal forms of over a dozen rigid cavitands—namely, **H,H,CH$_2$**, **H,Me,CH$_2$**, **Me,H,CH$_2$**, **Me,Me,CH$_2$**, **Br,Me,CH$_2$**, **Me,Et,SiMe$_2$**, **Me,i-Bu,CH$_2$**, and more[9,43]—are, in fact, intrinsically 0D porous molecular solids due to the inability of these shape-persistent macrocycles to efficiently pack in the crystalline state.[9] In terms of ensuring porosity, it appears that most any shape-persistent cavitand will be intrinsically porous, provided the peripheral functional groups cannot fill the intrinsic bowl of neighboring cavitands (*e.g.*, in **Me,Et,CH$_2$**). The precise size/shape of the observed 0D pores, however, are not entirely predictable; they are dictated, in part, by the shape of the intrinsic cavitand cavity, but they are also largely affected by the specific crystal packing. Thus, the microcavities (0D pores) in the aforementioned structures vary from ~28−115 Å^3 and can be even larger.[9] As porous solids, at least some of these materials (and, likely, most) can trap small molecules or monatomic gases within their intrinsic 0D pores, without significantly influencing crystal packing. For example, the CH_2Cl_2@**H,Me,CH$_2$** solvate is isostructural to its empty crystal form, and preliminary studies have revealed that **H,Me,CH$_2$** can selectively trap gases such as propene and dimethyl ether.

Among the more interesting of the 0D porous cavitands are those that possess dimethylsilyl bridges (Scheme 1, Y = $SiMe_2$). Though the microcavities are small, and the porosity is low (ε < 4%), the microcavity sizes/shapes are not much influenced by crystal packing, as the upper rim of the intrinsic cavitand cavity is defined almost completely by the dimethylsilyl bridges. For instance, although the crystal packings of empty **Me,Et,SiMe$_2$**[9] and **Me,H,SiMe$_2$** (reported here) are quite different, each possesses ~28 Å^3 intrinsic cavities of suitable size for very small molecules and monatomic gases. We previously reported that crystallization of **Me,Et,SiMe$_2$** from chloroform under ambient conditions gave the partial hydrate, xH$_2$O@**Me,Et,SiMe$_2$**, that is isostructural to empty **Me,Et,SiMe$_2$**.[9] Crystals of xH$_2$O@**Me,Et,SiMe$_2$** could be dehydrated in a single-crystal-to-single-crystal (SC → SC) fashion at elevated temperatures without deterioration in crystal quality, illustrating that **Me,Et,SiMe$_2$** is permeable to water. Also, in line with Cram's elegant studies concerning the binding properties of cavitands in solution,[39c] it was shown that **Me,Et,SiMe$_2$** captures Freon-41 (CH_3F, bp = −78 °C) from chloroform. As in the case of xH$_2$O@**Me,Et,SiMe$_2$**, the $x$$CH_3F$@**Me,Et,SiMe$_2$** clathrate is isostructural to the empty crystal form; bulk crystalline $x$$CH_3F$@**Me,Et,SiMe$_2$** loses Freon over a period of days at room temperature. Lastly, a single crystal of empty **Me,Et,SiMe$_2$** was subjected to 35 bar of CO_2 at room temperature for a period of 6.5 days, after which structure determination revealed the presence of 0.20 equiv of CO_2 within the intrinsic cavitand cavity. Clearly, 0D porous **Me,Et,SiMe$_2$** is permeable to small gases, despite there being no obvious mechanism for guest diffusion through the crystal.

We hypothesized that the gas permeability of **Me,Et,SiMe$_2$**, albeit low, may be in part due to the presence of the ethyl feet (Scheme 1, R′ = CH_2CH_3) and their position near the mouth of the intrinsic cavity in the crystal structure of empty **Me,Et,SiMe$_2$**. Though the structure exhibited no obvious disorder of these ethyl substituents, it is nonetheless conceivable that ethyl group dynamics facilitate gas exchange in these crystals. Thus, we hypothesized that **Me,H,SiMe$_2$**, lacking the ethyl feet, may exhibit higher kinetic barriers to guest sorption/desorption and thereby improved confinement properties relative to **Me,Et,-SiMe$_2$** (Scheme 2). What is more, stereopure *rccc*-**Me,Et,SiMe$_2$** is

Scheme 2. Qualitative Reaction Coordinate Diagram for the Sorption/Desorption of CO_2 by Solid, 0D Porous Cavitands Me,Et,SiMe$_2$ and Me,H,SiMe$_2$, Highlighting the High Barrier to Exchange That May Be Exploited for Confinement Purposes[a]

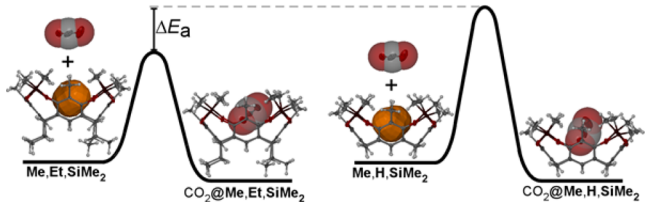

[a]Though the pores/microcavities are relatively inaccessible in both materials, it was hypothesized that CO_2 (and other gas) sorption/desorption would be slower in **Me,H,SiMe$_2$**, due to the absence of the flexible, potentially dynamic ethyl substituents.

available only in low yield, the chemistry giving also the *rcct*-**Me,Et,SiMe$_2$** stereoisomer which readily forms solid solutions with *rccc*-**Me,Et,SiMe$_2$**. **Me,H,SiMe$_2$**, however, has no stereoisomers and is easily synthesized in two steps, in good overall yield, from commodity chemicals (2-methylresorcinol, formaldehyde, dichlorodimethylsilane).[40]

2. Empty, 0D Porous Me,H,SiMe$_2$, Its Isostructural Solvates, and Host Flexibility. Single crystals of the empty **Me,H,SiMe$_2$** apohost can be obtained by thermal sublimation of the dry material under dynamic vacuum. Structure determination by single crystal X-ray diffraction (SCXRD, 100 K, Figure 1) reveals that the molecules pack in a rather unremarkable fashion. The crystals adopt a monoclinic $C2/c$ packing arrangement (Z = 8) and consist of a seemingly as-close-as-possible arrangement of cavitand layers in the *bc*-plane. The layers are made up of polar, canted cavitand columns that are packed in pairs, and the paired columns are arranged in an antiparallel fashion, related by an inversion center. Adjacent layers are also related by inversion. The 100 K unit cell volume averages 8230(10) Å^3, as determined for several crystals. Though the molecules of **Me,H,SiMe$_2$** are close-packed, the bowl-shaped cavitands preserve discrete, empty microcavities (0D pores) of approximately 28 Å^3 (V_{cav}, Table 1, pore probe radius = 1.4 Å), corresponding to a porosity (ε) of 2.7%.[44] Electron density analysis (SQUEEZE[45]) reveals

DOI: 10.1021/jacs.5b11395
J. Am. Chem. Soc. 2016, 138, 4377−4392

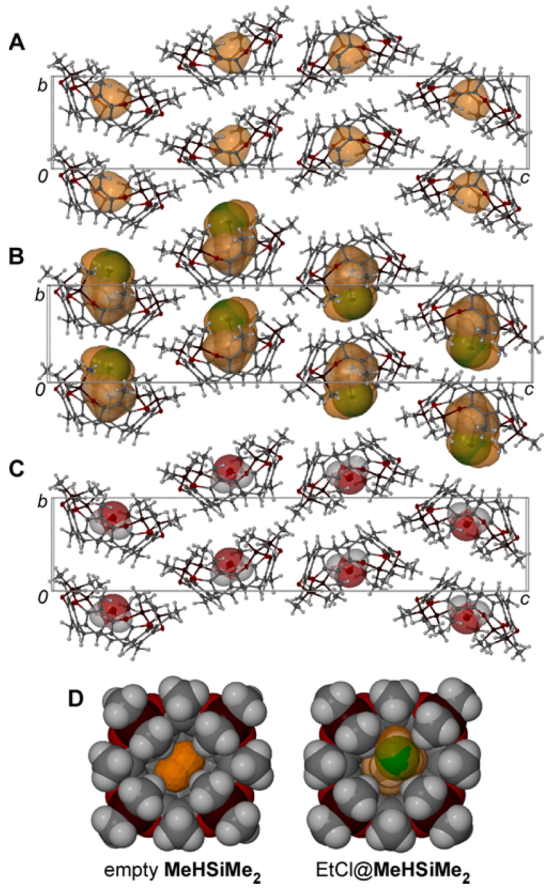

Figure 1. Isostructural crystal packings (at 100 K) of the following: (A) Empty, 0D porous **Me,H,SiMe$_2$**, illustrating the unoccupied 28 Å^3 microcavities. V_{cell} = 8230 Å^3. (B) The most expanded of the isostructural *x*(guest)@**Me,H,SiMe$_2$** ($x \leq 1$) clathrates, CH_3CH_2Cl@**Me,H,SiMe$_2$**. V_{cell} = 8446 Å^3 (100 K), $\Delta\tau$(avg) = 11°. (C) The xH_2O@**Me,H,SiMe$_2$** ($x < 0.4$) partial hydrate. For clarity, only one layer of the structure is shown. (D) Spacefill models of the empty and CH_3CH_2Cl-occupied **Me,H,SiMe$_2$** cavitands as viewed from the top of the bowls. Probe-accessible cavity volumes (28 and 76 Å^3, respecitively; 1.4 Å probe) are depicted in orange.

that freshly prepared crystals are truly empty. Moreover, thermogravimetric analysis (TGA) of empty **Me,H,SiMe$_2$** reveals no mass loss whatsoever up to the point of sublimation, which onsets at about 300−310 °C and reaches its maximum rate at about 395(12) °C (see Supporting Information (SI), heating rate = 5 °C/min.).

Importantly, the estimated cavity volume in **Me,H,SiMe$_2$** is unusually dependent upon the radius of the probe used to map the pore. Whereas a 1.4 Å diameter pore probe yields a V_{cav} = 28 Å^3, the value jumps to 49 Å^3 when a 1.2 Å probe is used, as the smaller diameter probe is able to escape the confines of the dimethylsilyl bridges (see SI) yet is confined by the adjacent molecule in the structure. Thus, it can be understood that very minor changes in atomic positions of the dimethyl silyl groups will have large consequences on the apparent cavity (0D pore) volume (Figure 1D). The room temperature structure of empty **Me,H,SiMe$_2$** was also determined (Table S4), and other than increased atomic displacement parameters and the anticipated expansion of the unit cell, there appear to be few material differences between the low temperature and room temperature structures, including the V_{cav} values.

In contrast, when **Me,H,SiMe$_2$** is crystallized by evaporation from certain small molecule organic solvents, it forms 1:1 solvent@**Me,H,SiMe$_2$** clathrates (e.g., solvent = CH_3I, CH_3CN, CH_3NO_2). The compositions of all clathrates were established by single crystal X-ray diffraction (SCXRD), and thermal gravimetric analysis (TGA), or tandem TGA-mass spectrometery (TGA-MS), and ^{1}H NMR spectroscopic analysis (where applicable) of the bulk samples. Except where noted, the results from the three techniques roughly concur with the SCXRD measurement. Table 1 summarizes compositional, structural, NMR, and TGA data for *x*(guest)@**Me,H,SiMe$_2$** ($x \leq 1$) clathrates, arranged by the boiling point of the guest. Table S4 contains summary crystallographic data for structure determinations by SCXRD. Notably, all solvates adopt essentially the same crystal packing as the empty form, with the solvents simply occupying the otherwise empty cavitand cavities. Thus, the solvates may be regarded as guest-loaded forms of the thermodynamically stable 0D porous **Me,H,SiMe$_2$** phase. For instance, the 100 K unit cell volume of CH_3CN@**Me,H,SiMe$_2$** (V_{cell} = 8244(2) Å^3)—the clathrate of the smallest of these organic solvents—is nearly indistinguishable from empty **Me,H,SiMe$_2$**, despite a doubling of the cavity volume (V_{cav}) from 28 to 64 Å^3 (6.2% of the crystal) to accommodate the CH_3CN molecule, which has a volume of 44 Å^3 (V_{guest}). The CH_3CN is efficiently packed within the **Me,H,SiMe$_2$** cavity, occupying approximately 69% of the available volume, the so-called cavity packing fraction (PF_{cav}, Table 1). Notably, the eight included molecules of acetonitrile require ~494 Å^3 of space in the close packed crystal structure of pure acetonitrile (at 100 K), yet their enclathration by 0D porous **Me,H,SiMe$_2$** (Z = 8) leads to no statistically meaningful change in the unit cell volume. Remarkably, the formal doubling of the **Me,H,SiMe$_2$** cavity volume entails only a slight outward swinging of the O−Si−O linkages such that the angles between the planes defined by the O−Si−O linkages and the plane defined by the upper rim oxygen atoms of the pseudo 4-fold symmetric cavitand (angle τ in Scheme 1) are all slightly more acute. For example, the average τ angle ($\Delta\tau$(avg)) in CH_3CN@**Me,H,SiMe$_2$** is 8.4° smaller than that for the empty phase, apparently doubling the cavitand cavity volume, but resulting in little to no change in the unit cell volume.

The unit cells of the isostructural 1:1 clathrates of slightly larger solvents (CH_3I, CH_3NO_2), however, are slightly expanded as compared to empty **Me,H,SiMe$_2$** (Tables 1, S4). Moreover, room temperature crystallization of **Me,H,SiMe$_2$** from solvents that are larger (CH_2Cl_2 [V_{guest} = 59 Å^3] and $BrCH_2Cl$ [V_{guest} = 64 Å^3]) consistently leads to only partially occupied solvates, 0.85CH_2Cl_2@**Me,H,SiMe$_2$** and 0.74$BrCH_2Cl$@**Me,H,SiMe$_2$** by SCXRD, despite the large excess of these potential guests as the solvent. The resulting crystals are formally solid solutions of occupied and empty cavitands. For example, a single crystal of the $BrCH_2Cl$ clathrate gave a refined occupancy of 0.74(1), whereas ^{1}H NMR and TGA of the bulk phase gave values of 0.62 and 0.63 equiv per cavitand, respectively. Similarly, a single crystal of the CH_2Cl_2 clathrate gave a refined occupancy of 0.85(1). ^{1}H NMR and TGA of the bulk phase gave values of 0.84 and 0.97 equiv per cavitand, respectively. The differences in occupancies determined by these analytical methods illustrate the challenges involved in accurately quantifying the exact amount of guest present in partial occupancy clathrates. In 0.85CH_2Cl_2@**Me,H,SiMe$_2$**, the ^{1}H NMR analysis seems to validate the occupancy determination by SCXRD. The occupancy observed by TGA, however, appears to be artificially large. In our experience, this can often be attributed to

DOI: 10.1021/jacs.5b11395
J. Am. Chem. Soc. 2016, 138, 4377−4392

Table 1. Summary of Compositional, Structural, and Thermal Analysis Data for Isostructural Clathrates x(Guest)@Me,H,SiMe$_2$ ($x \leq 1$) and CH$_3$CCH@Me,H,SiMe$_2$·2CHCl$_3$, Arranged by Boiling Point of the Guest[a]

			fractional occupancy (SCXRD/other)					TGA			
guest	bp (°C)	V_{guest} (Å^3)	as prepared (day = 0)[b]	day ≥ 7[b,e]	V_{cav} (Å^3)	PF$_{cav}$	V_{cell} (Å^3)	wt %$_{th}$	wt %$_{exp}$	T_{max} (°C)	$T_{max} - T_{bp}$ (°C)
none	n/a	n/a	0[n]	n/a	28	0	8230(10)	0	0	395(12)[p]	n/a
N_2	−196	25	0.34(2)[f]/0.20[g]	0.23(2),[h] 0.14(5)[h]	31	0.80	8244(3)	1.1	0.7	>100	>296
Ar	−186	28	0.61(4)[f,h]/0.58[g]	0.29[g]	36	0.78	8219(3)	3.1	2.9/1.5[e]	118	315
CH_4	−162	28	0.79(6)[f,h]/0.78[g]	0.84(8),[h] 0.73[g]	62	0.45	8254(2)	1.6	1.6/1.5[e]	149	311
Kr	−153	35	0.50(4);[f] 0.48[g]	0.44[g]	nm	nm	8235(2)	5.2	5.0/4.6[e]	191	334
Kr	−153	35	0.51(3)[f,h]	0.07(1)[e,h]	nm	nm	8231(4)	5.4	nm[m]	nm	nm
Xe	−108	42	0.79(2)[f]/0.83[g]	nd	66	0.64	8274(2)	11.9	12.4	185	293
Xe	−108	42	0.77(3)[f]	0.79(2)	66	0.64	8261(13)	11.6	nm[m]	nm	nm
C_2H_4	−104	40	0.61(4);[f,h] 0.69[g]	0.65(4),[h] 0.69[q]	60	0.67	8240(7)	2.2	2.5/2.5[q]	172	276
C_2H_4	−104	40	0.062(9)[c,d]	0.037(1)[c,d]	nd	nd	nd	nd	nd	nd	nd
C_2H_6	−89	45	0.58(1);[f,h] 0.63[g]	0.58(1),[h] 0.60[g]	68	0.65	8278(9)	2.2	2.4/2.3[e]	178	267
C_2H_6	−89	45	0.72(2)[f,h]/0.76[g]	nd	67	0.67	8270(1)	2.7	2.9	130	219
C_2H_6	−89	45	0.056(5)[c,d]	0.055(4)[c,d]	nd	nd	nd	nd	nd	nd	nd
HC≡CH	−84	34	0.055(4)[c,d]	0	nd	nd	nd	nd	nd	nd	nd
CH_3F	−78	32	0.80(4)/0.82[g]	0.37,[h] 0.24(1)[h]	51	0.63	8218(2)	3.4	3.5	203	281
CH_3F	−78	32	0.51(5)[c,d]	0.27(6)[c,d]	nd	nd	nd	nd	nd	nd	nd
CO_2	−78[o]	32	0.46(6)[f,h]/0.39[g]	0.36(6)[f,h]/0.36[g,q]	61	0.52	8214(1)	2.6	2.2/2.0[q]	109	187
CO_2	−78[o]	32	0.42(1)[f,h]/0.54[g]	0.36(2)[f,h]/0.48[g,q]	64	0.50	8214(1)	3.0	2.7[q]	112	190
H_2S	−60	31	0.85(4)/1.2[g,m]	nd	52	0.60	8216(3)	4.2[j]	5.1[m]	157	217
CH_3Cl	−24	44	0.90(4)[i]/1.0,[g] 0.98(1)[k]	nd	62	0.71	8280(2)	6.2[j]	6.4	233	257
CH_3Cl	−24	44	1.0[c,d]	0.84[c,d]	nd	nd	nd	nd	nd	nd	nd
CH_3OCH_3	−24	53	0.82(4);[f] 0.40(2)[c,d]/0.94[g]	0.35(1)[c,d]	80	0.66	8349(1)	4.7	5.3	162	186
$CH_3C{\equiv}CH$	−23	51	1.02(2),[i,l] 1.0[c,d]	0[c,d]	74	0.69	5003(2)[l]	nm[l]	nm[l]	nm	nm
CH_3Br	4	49	0.91(4)[i]	nd	75	0.65	8307(2)	11.0[j]	nm[m]	230	226
CH_3SH	6	46	0.83(4)	nd	72	0.64	8278(1)	nd	nd	nd	nd
CH_3CH_2Cl	12	61	0.95(2)[f,i]	nd	76	0.80	8446(1)	nd	nd	nd	nd
CH_3CH_2Cl	12	61	1.0,[c,d] 1.0[g]	1.0[c,d]	nd	nd	nd	7.7	7.6	158	146
CH_2Cl_2	40	59	0.85(1), 0.84[d]/0.97[g,m]	nd	74	0.80	8378(1)	8.4	9.7[m]	179	139
CH_3I	42	53	0.95(3)[i]	nd	77	0.69	8371(1)	15.6[j]	nm[m]	210	168
CH_3OH	65	37	0.67(8), 0.56[d]/0.89[g]	nd	52	0.71	8230(1)	2.8	3.6	160	95
$BrCH_2Cl$	68	64	0.75(1), 0.62[d]/0.63[g]	nd	82	0.78	8404(1)	11.7	9.6	177	109
EtOH	78	54	0.13(4), 0.11[d]	nd	nm	nm	8241(2)	0.8	trace	nm	nm
CH_3CN	81	44	0.96(3)[i], 0.96[d]	nd	64	0.69	8244(2)	5.1[j]	nm[m]	nm	nm
CH_2Br_2	97	69	0,[b] 0.08[d]/0.10[g]	nd	–	–	–	2.0[d]	2.2	115	18
H_2O	100	18	0.20(2)[n]/0.29(2)[n]	nd	28	0.65	8222(27)	<0.5	trace	nm	nm
CH_3NO_2	101	51	0.95(5),[i] 0.87[d]	nd	69	0.74	8277(2)	7.4[j]	nm[m]	nm	nm
I_2	113[o]	60	0.06(1)	0.06(1)/0.06[g]	nm	nm	8242(1)	2.3	2.4	nd	nd

[a] T_{max} = temperature of maximum rate of guest loss (5 °C/min heat rate; as synthesized samples). $T_{max} - T_{bp}$ = difference between T_{max} and the normal boiling point of the guest. Nd = not determined. Nm = not meaningful (see SI). [b] Unless otherwise indicated, occupancy determined by SCXRD and crystals grown at room temperature (RT) by either evaporation from the included solvent, or from saturated $CHCl_3$ solutions of **Me,H,SiMe$_2$** treated with guest: excess CH_3OH, CH_3CH_2OH, gas at atmospheric pressure, or excess I_2. Different batch preparations appear on different lines (ln). [c] Powder samples were obtained by passing the gas of interest through a $CHCl_3$ solution of **Me,H,SiMe$_2$** until dry. [d] Occupancies determined by ^{1}H NMR. [e] Crystals left at ambient conditions (or in desiccator) for 1 week, or for the time/temperature as follows: N_2, 54 h, plus 9.5 days (dry), respectively; Ar, 3 days (dry), CH_4, 5 days (dry); Kr, 3 days (ln 1), 14 days at 100 °C (ln 2); Xe (ln 2), 112 days; C_2H_4 (ln 1), 11 days; C_2H_6 (ln 1), 11 days; CO_2, 10 days; CH_3F (ln 1), 146 days, then 4 days at 150 °C. [f] Precipitated at RT (dry $CHCl_3$) under an undetermined elevated pressure of gas, or specific pressures as follows: N_2, 80 bar; Ar, 80 bar; CH_4, 36 bar; Kr, 9.8 bar (ln 1); Xe, 9.8 bar (ln 1); C_2H_4, 9.8 bar (ln 1); C_2H_6, 9.8 bar (ln 1); CO_2, 25 bar (ln 2); CH_3OCH_3, < 5.9 bar; CH_3CH_2Cl, < 1.3 bar; see SI. [g] Occupancy estimated by TGA. [h] Same crystal. [i] Fixed at 1.0 for SCXRD refinement. [j] 100% occupancy. [k] Crystal from EtOAc. [l] CH_3CCH@**Me,H,SiMe$_2$**·2$CHCl_3$; readily loses solvent and gas at RT. [m] Wt% not meaningful; guest loss induces cosublimation of **Me,H,SiMe$_2$** in open TGA pans. [n] Same crystal; partial hydrate (0.20 equiv) emptied at 150 °C (0 equiv) and rehydrated (0.29 equiv). [o] Sublimation. [p] T_{max}(esd) of sublimation; onset temperature is ca. 310 °C. [q] Mass loss after: C_2H_4, 4 days; CO_2, 7 days (ln 1), 8 days (ln 2).

cosublimation of the host that occurs concomitantly with guest loss; the effect can be minimized by loading the TGA samples into DSC pans that contain pinholes to allow guest escape. Additionally, we have observed that occupancy measurements by NMR can be artificially low for samples where the solubility of the guest in the NMR solvent is low (e.g., gaseous guests, *vide infra*). Means of estimating errors by SCXRD are discussed in the SI.

The observed unit cell volumes and conformational $\Delta\tau$ angles of the host generally correlate with the volume of the solvent: the

DOI: 10.1021/jacs.5b11395
J. Am. Chem. Soc. 2016, 138, 4377−4392

cavitand shows a remarkable ability to expand its molecular cavity, from 28 Å^3 to an apparent maximum of nearly 80 Å^3 (a 285% expansion, Figure 1D) to accommodate the largest guests (e.g., CH_2Cl_2, and CH_3CH_2Cl (*vide infra*)). Moreover, via unit cell expansions and subtle changes in the crystal packing, **Me,H,SiMe$_2$** also shows some ability to accommodate modest protrusions of the enclathrated guests from the upper rim of the cavity. The 100 K unit cell appears to accommodate expansion up to a maximum of about 8440 Å^3 (ΔV_{cell} = 210 Å^3, 2.5%). For example, the 100 K unit cell of a single crystal of $0.85CH_2Cl_2$@**Me,H,SiMe$_2$** (V_{cell} = 8378(1) Å^3, Figure 1)—formally, an 85:15 solid solution of occupied and empty cavitands—is only 1.8% larger than the empty, 0D porous **Me,H,SiMe$_2$** apohost (ΔV_{cell} = 148 Å^3). The extent of crystal expansion is minimal considering that, on average per unit cell, 6.8 molecules of CH_2Cl_2 (6.8 × 59 Å^3 = 401 Å^3, which require 558 Å^3 of space in pure crystalline CH_2Cl_2 at 153 K)[46] have been introduced into the material. In fact, the partial occupancy of CH_2Cl_2 suggests that this guest approaches the upper volume/shape limit of what can be tolerated by the empty-like monoclinic phase of **Me,H,SiMe$_2$**.

Seeking to further explore the cavity limits, **Me,H,SiMe$_2$** was also crystallized at room temperature by evaporation from even larger solvents (Tables 1, S4 and Figure S68), CH_2Br_2 (69 Å^3), chloroform ($CHCl_3$, 72 Å^3), and ethyl acetate (EtOAc, 85 Å^3). Crystallization from dibromomethane yields single crystals that appear, by SCXRD, to be free of the solvent, but by ^{1}H NMR and TGA the samples appear to contain up to 0.1 equiv of the solvent (Table 1). Remarkably, the small yet continuous increase in the solvent volume on going from CH_2Cl_2 (59 Å^3), to $BrCH_2Cl$ (64 Å^3), to CH_2Br_2 (69 Å^3) has a dramatic effect on the ability of **Me,H,SiMe$_2$** to enclathrate these solvents at room temperature, giving $x \approx 0.85$, 0.74, and 0.1 x(solvent)@**Me,H,SiMe$_2$** clathrates, respectively.

Because the solvents are simply too large to be accommodated by **Me,H,SiMe$_2$** or its monoclinic crystal form, crystallization from $CHCl_3$ or EtOAc results in empty **Me,H,SiMe$_2$** under rigorously dry conditions. When no drying precautions are taken, crystallization from these solvents results in partial hydrates $x(H_2O)$@**Me,H,SiMe$_2$** (x < 0.4, Figure 1). Importantly, the appearance of water within the hydrophobic cavities of **Me,H,SiMe$_2$** illustrates the ability of **Me,H,SiMe$_2$** to scavenge even noncomplementary, hydrophilic guests in the absence of more appropriate small molecules. Moreover, as water is relatively small (18 Å^3), the structures of the $x(H_2O)$@**Me,H,SiMe$_2$** partial hydrates are indistinguishable from empty **Me,H,SiMe$_2$** with the exception that the oxygen atom of the partial occupancy water molecule is clearly identifiable in the difference electron density map. Its deep position in the cavity (d = 0.29(4) Å, defined in Scheme 1) and the O···C(arene) intermolecular contact distances are suggestive of O−H··· arene(π)hydrogen bonds,[47] such as those studied in sodium salts of calix[4]arenesulfonate.[48]

Notably, the $x(H_2O)$@**Me,H,SiMe$_2$** crystal structures we obtained are somewhat different from the only other reported crystal structure of **Me,H,SiMe$_2$**, that of the room temperature "monohydrate" (R_1 = 9.1%) previously described by Lara-Ochoa et al.[40] First, the former was reported to have crystallized from CH_2Cl_2, which is contrary to our observation that crystallization from CH_2Cl_2 gives the solvate $0.85CH_2Cl_2$@**Me,H,SiMe$_2$**. Additionally, the former structure determination models two oxygen atom sites, whereas we find no evidence of water disorder in the partial hydrates. Moreover, the current structure determinations are of much higher quality.

Seeking to further explore the ability of **Me,H,SiMe$_2$** to enclathrate hydrophilic guests, **Me,H,SiMe$_2$** was precipitated from chloroform using a large excess of methanol (MeOH) and ethanol (EtOH), yielding single crystals of the partially occupied solvates 0.67(MeOH)@**Me,H,SiMe$_2$** and 0.13(EtOH)@**Me,H,SiMe$_2$**, respectively (Tables 1, S4 and Figure S68). Though MeOH and EtOH (V_{guest} = 37 and 54 Å^3, respectively) solvents are certainly small enough to be accommodated by the monoclinic phase of **Me,H,SiMe$_2$**, they are isolated as partial occupancy clathrates, illustrating the greater affinity of **Me,H,SiMe$_2$** for hydrophobic guests.

Clearly, the observation of partially occupied solvates alludes to a rather impressive volume, shape, and chemical enclathration selectivity of **Me,H,SiMe$_2$** and its monoclinic crystalline phase. Apparently, in solution at room temperature, the cavities of **Me,H,SiMe$_2$** are only partially occupied (or not at all) by molecules of solvent if the solvent is too large to easily penetrate the molecular cavity. Thus, partial or complete solvent exclusion seems to arise for solvent molecules of nonlinear shape and a volume greater than about ca. 65 Å^3. An alternative possibility is that the process of crystal nucleation and growth may be selective with respect to the ratio of occupied and unoccupied cavitands incorporated into the crystal such that there is an effective upper limit on the expanded average unit cell volume that can be achieved by **Me,H,SiMe$_2$** solid-solutions in the low-energy, close-packed, monoclinic, packing arrangement, the limit being about 8446 Å^3 when measured at 100 K [for CH_3CH_2Cl@**Me,H,SiMe$_2$** (Table 1), the largest volume guest complexed in this study].

3. Gas Capture by Me,H,SiMe$_2$. The aforementioned behavior—namely, the 0D porous structure of empty **Me,H,SiMe$_2$**, the isostructural solvates, and the volume/shape/chemically selective enclathration properties—prompted our exploration of the potential for **Me,H,SiMe$_2$** to selectively capture and confine gases. The following sections detail various experiments, observations, and the corresponding conclusions that can be drawn. Table 1 gives a summary of the clathrate syntheses, and compositional, structural, and NMR and/or TGA data for the isostructural series of x(gas)@**Me,H,SiMe$_2$** ($x \leq 1$) clathrates and one isolated mixed gas/solvent clathrate, namely CH_3CCH@**Me,H,SiMe$_2$**·$2CHCl_3$, arranged by the boiling point of the enclathrated gas. All clathrates (gas clathrates, solvent clathrates, and one I_2 clathrate) were characterized at least by single crystal X-ray diffraction (SCXRD), TGA, and ^{1}H NMR spectroscopy (where applicable), except for $0.8(CH_3SH)$@**Me,H,SiMe$_2$**, which was characterized only by SCXRD, and $0.05(C_2H_2)$@**Me,H,SiMe$_2$**, which was characterized only by ^{1}H NMR spectroscopy. Several gas clathrates (those of Ar, Kr, Xe, C_2H_6, and CO_2) were additionally characterized by tandem TGA-mass spectrometry (TGA-MS), and the analyses clearly show mass spectral signatures of the gas appearing concomitantly with mass loss (Figures S14, S19, S24, S37, S51, respectively). Details of sample preparations and characterization data of the various batch samples are provided as SI.

3.1. Capture of (Protic) Gases: ^{1}H NMR Studies. To initially probe the ability of **Me,H,SiMe$_2$** to form stable gas clathrates, various protic gases were passed through chloroform solutions of **Me,H,SiMe$_2$** until the solvent had completely evaporated (the "Bubbling to Dryness" method). The resulting solids were then rigorously flushed with nitrogen and were subsequently analyzed by ^{1}H NMR spectroscopy. The spectra showed unequivocally (Table 1, experiments performed in triplicate) that 1 equiv of chloroethane (CH_3CH_2Cl, Figures S64–S65), chloromethane

DOI: 10.1021/jacs.5b11395
J. Am. Chem. Soc. 2016, 138, 4377–4392

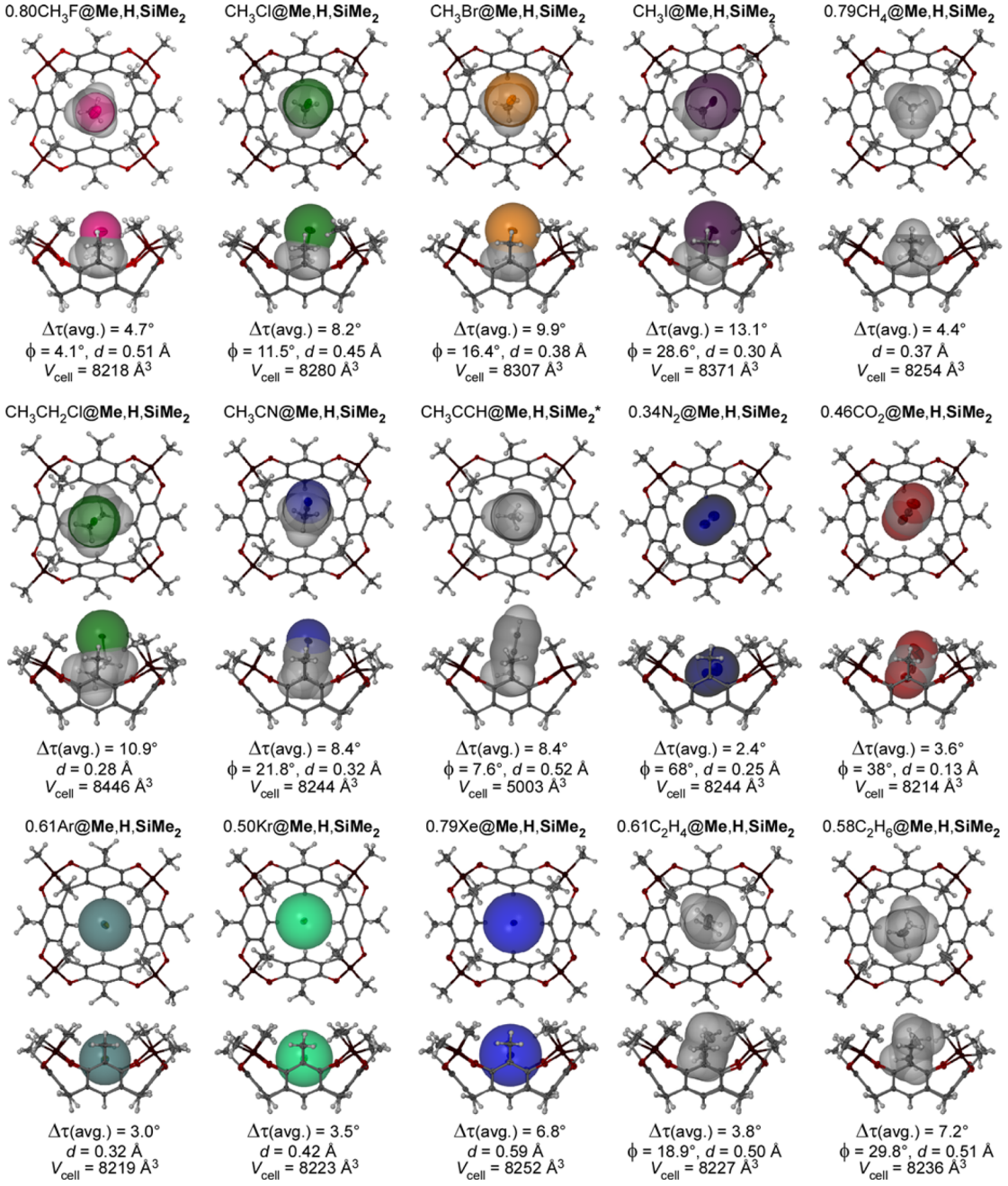

Figure 2. Thermal ellipsoid plots of selected isostructural *x*(gas/solvent)**@Me,H,SiMe$_2$** ($x \leq 1$) clathrates (at 100 K, 50% probability level), along with summary structural parameters V_{cell}, $\Delta\tau$(avg), ϕ, and *d*, defined in the text. Other clathrates are depicted in Figure S68. The CH$_3$CCH**@Me,H,SiMe$_2$** complex is taken from the structure of CH$_3$CCH**@Me,H,SiMe$_2$**·2CHCl$_3$. (Colors: gray, carbon; red, oxygen; maroon, silicon; white, hydrogen; green, chlorine; dark blue, nitrogen; orange, bromine; purple, iodine; pink, fluorine; teal, argon; light green, krypton; royal blue, xenon.)

(CH$_3$Cl, Figures S53–S54), and propyne (CH$_3$CCH, Figure S59) were captured by the cavitand under these conditions. Lesser, but significant, amounts of fluoromethane (CH$_3$F, 0.51(3) equiv, Figure S45) and dimethyl ether (CH$_3$OCH$_3$, 0.40(2) equiv, Figure S56) were captured, and very small amounts of ethane (CH$_3$CH$_3$, 0.056(5) equiv, Figure S34), ethylene (CH$_2$═CH$_2$, 0.062(9) equiv, Figure S27), acetylene (C$_2$H$_2$, 0.055(4) equiv, Figure S43), and possibly methane (trace) were captured. Notably, there was no evidence for the capture of propane or propene under these conditions.

As a preliminary probe of the kinetic stability of the gas clathrates, the resulting solids were analyzed again by ^{1}H NMR spectroscopy after 7 days of being exposed to room temperature conditions in open vials. The results showed that, with the exception of methane, acetylene (Figure S44), and propyne, even extremely volatile gases such as CH$_3$F (bp = −78 °C, Figure S46), ethane (bp = −89 °C, Figure S35), ethylene (bp = −104 °C, Figure S28), and dimethyl ether (bp = −24 °C) (Figure S57) were largely or completely retained by the host after 1 week (Table 1). Notably, propyne, 1 equiv of which was initially captured by **Me,H,SiMe$_2$**, was completely missing from the solid after 7 days (Figure S60), an observation seemingly at odds with the ability of **Me,H,SiMe$_2$** to confine much more volatile and less effectively captured gases.

3.2. x(Gas)@Me,H,SiMe$_2$ Single Crystals. 3.2.1. Preparation and Characterization. To extend the investigation to nonprotic

DOI: 10.1021/jacs.5b11395
J. Am. Chem. Soc. 2016, 138, 4377−4392

gases, and probe the structural factors that influence enclathration selectivity and kinetic stability, numerous isostructural x(gas)@**Me,H,SiMe$_2$** ($x \leq 1$) clathrates (and an I_2 clathrate) were prepared and their structures determined by SCXRD (Table S4, Figure 2). Several of the gas clathrates could be prepared in single crystal form by simply passing the gas of interest, at atmospheric pressure, through a saturated solution of **Me,H,SiMe$_2$** (0.104 M) in chloroform until slight precipitation of clathrate occurred. The vials were then capped, warmed slightly to redissolve the precipitate, and set aside for crystal growth at room temperature. For gases that are only weakly complexed by **Me,H,SiMe$_2$** (typically, low boiling point gases), more forcing growth conditions were employed. Crystals of such gas clathrates were grown by one of two methods: (i) A general, elevated pressure method: The gas was cryogenically liquefied in a graduated cylinder. The cold, liquified gas was then sealed in a Teflon-lined digestion bomb alongside a dry, saturated solution of **Me,H,SiMe$_2$** in chloroform. Crystal growth was allowed to occur over a period of days. In this way, the total pressure of the gas in the digestion bomb could only be loosely estimated. (ii) A defined pressure method: A custom stainless steel vessel, fitted with a pressure gauge and containing a vial of a dry, saturated chloroform solution of **Me,H,SiMe$_2$**, was charged with and held under a constant pressure of the gas (±0.1 bar), inducing crystallization. A partial I_2 clathrate, 0.06(2)I_2@**Me,H,SiMe$_2$**, was synthesized by adding a modest excess of I_2 to a saturated chloroform solution of **Me,H,SiMe$_2$** and allowing crystals to grow by slow evaporation over a few days. Apparently, **Me,H,SiMe$_2$** has a relatively low affinity for I_2, likely due to its large size (60 Å^3) which is comparable to CH_2Br_2. Additional details are available in the Supporting Information.

Figure 2 depicts thermal ellipsoid plots and some pertinent structural features (d, $\Delta\tau$ (avg), and ϕ, defined in Scheme 1) of 15 of the isostructural x(guest)@**Me,H,SiMe$_2$** complexes characterized by SCXRD. In all cases, the guest occupancies were estimated by single crystal X-ray diffraction, and TGA and ^{1}H NMR obtained on the bulk samples were generally in accord with the X-ray results (Table 1, with specific exceptions as discussed). Moreover, the X-ray structures of these isostructural gas clathrates are of such quality that one can place some confidence in the accuracy and precision of the guest occupancies as determined by refinement of the diffraction data (estimated ±3%). Atom occupancy refinement[49] and electron density analysis (SQUEEZE[45]) enabled determination of the guest occupancy, and estimated standard deviations of the occupancies are based on discrepancies between these methods (Table S1). The accuracy of the occupancy measurements were generally validated by TGA (Table 1; see SI). Where refined occupancies were within 3 esds of 1.0 equiv per cavitand, the guest was refined at full occupancy.

In general, SCXRD analysis of multiple crystals from the same batch preparation gave identical or very similar occupancies, within error, indicating a roughly uniform occupancy among the individual crystals in a given batch preparation. Moreover, the gas occupancies were approximately reproducible, batch-to-batch, when crystallized under the same gas pressures (see SI). It is as yet unknown whether the gas composition is homogeneous throughout the partial occupancy crystals, but it would stand to reason that, for crystals grown under constant pressure, it may be. The thermal ellipsoid plots of the individual encapsulated gas molecules are provided in the SI.

3.2.2. Comments on Selective Enclathration. The occupancies of the x(gas)@**Me,H,SiMe$_2$** ($x \leq 1$) clathrates obtained under the various preparation conditions are a reflection of the selectivity of the **Me,H,SiMe$_2$** molecule (and/or its 0D porous crystalline phase) for the various gases. The small cavity of **Me,H,SiMe$_2$** is able to bind the gases to varying degrees in $CHCl_3$ solution, a solvent that is too large to enter the cavity. Thus, as pointed out by James, a solution of **Me,H,SiMe$_2$** in $CHCl_3$ may be considered to be a porous liquid that may scavenge gases or other small molecules.[21] Binding of gases and small molecules by cavitands in solution is not new: Cram and co-workers observed that the related, more shallow cavitand **H,Me,SiMe$_2$** weakly binds CS_2, $CH_3C{\equiv}CH$, and even O_2 in $CHCl_3$ solution, though the association constant measured for CS_2 (the only one measured) was very small (K_a = 0.22 at 300 K).[50] Notably, despite specific efforts to observe complexation-induced shifts in ^{1}H NMR spectra, Cram and co-workers found no evidence for the complexation of CH_3I by **H,Me,SiMe$_2$** in $CHCl_3$, or, for that matter, CH_2Cl_2, H_2O, or CO_2. Nonetheless, we find that each of these guests is enclathrated by **Me,H,SiMe$_2$** when crystallized under the appropriate conditions.

The observed gas occupancies in the x(gas)@**Me,H,SiMe$_2$** ($x \leq 1$) clathrates depend on several factors, considering that, formally, the empty cavitand, the free gas, and the gas@cavitand complex establish an equilibrium in solution according to the association constant, K_a, for gas complexation in the solvent. Thus, the solubility of the gases (the Henry constant, k_H) in the solvent of crystallization plays an important role (Figure 3).

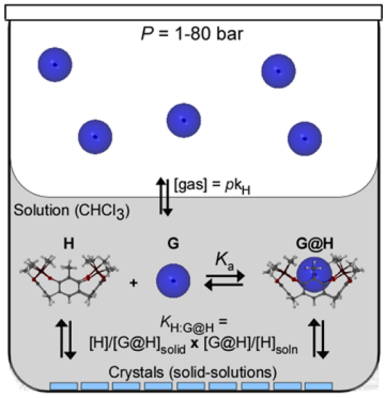

Figure 3. Schematic summarizing x(gas)@**Me,H,SiMe$_2$** clathrate syntheses. A saturated (104 mM), dry solution of **Me,H,SiMe$_2$** is treated/pressurized (P = 1−80 bar) with the gas of interest (blue). The equilibrium concentration of the free gas in solution depends on the pressure of the gas (p) and its solubility, given by its Henry coefficient (k_H). The gas occupancy, x, of the crystalline x(gas)@**Me,H,SiMe$_2$** solid solutions grown under these conditions depends on the solution gas binding constant (K_a) and the selectivity of the crystallization process ($K_{H:G@H}$) for incorporating empty **Me,H,SiMe$_2$** or gas@**Me,H,SiMe$_2$** species.

Increasing the pressure of the gas over the solvent increases the concentration of the free gas in solution according to Henry's Law ($P = k_H$[gas]). This, in turn, shifts the equilibrium toward the gas@**Me,H,SiMe$_2$** complex and gives rise to x(gas)@**Me,H,SiMe$_2$** ($x \leq 1$) clathrates with occupancies that increase with gas pressure. In this way, gas clathrates of nearly any gas that is capable of being accommodated by the 0D pores of **Me,H,SiMe$_2$** can be prepared; pressurizing solutions of **Me,H,SiMe$_2$** leads to precipitation of x(gas)@**Me,H,SiMe$_2$** clathrates of even the most volatile, weakly interacting gases (e.g., Ar, N_2, C_2H_6, *etc.*). The approach is similar to that used for

DOI: 10.1021/jacs.5b11395
J. Am. Chem. Soc. 2016, 138, 4377−4392

the growth of gas clathrates of C_{60}.[36] Importantly, it is conceivable that the crystal nucleation and/or growth process is selective toward incorporation of the empty **Me,H,SiMe$_2$** host or the gas@**Me,H,SiMe$_2$** complex, with a selectivity coefficient, $K_{H:G@H}$, that is not necessarily unity.

The gas occupancy trends observed in the preparation experiments can be explained as follows. **Me,H,SiMe$_2$** clearly exhibits the highest affinity for methylhalide (CH_3X) gases, owing to size/shape and electronic (dipole matching) complementarity of these gases to the tiny, polar molecular cavity (and the corresponding 0D pore). When nearly saturated solutions of **Me,H,SiMe$_2$** in chloroform were saturated with 1 atm of the following gases, isostructural x(gas)@**Me,H,SiMe$_2$** ($x \leq 1$) clathrates precipitated as large single crystals over a period of minutes to days: CH_3F ($x = 0.80(4)$), CH_3Cl ($x = 0.90(4)$), CH_3Br ($x = 0.91(4)$), CH_3SH ($x = 0.83(4)$), H_2S ($x = 0.85(4)$). The relatively high occupancies of the CH_3SH and H_2S clathrates are likely attributable, in part, to the relatively high solubility of these gases in chloroform.[51] That simply exposing solutions of **Me,H,SiMe$_2$** to these gases induces crystallization of the gas clathrate is a significant observation. The lattice energies of these x(gas)@**Me,H,SiMe$_2$** complexes are apparently greater than that of the isostructural empty, air-gas-occupied, or partial hydrate phases that could alternatively form. Thus, formation of significant amounts of the gas@**Me,H,SiMe$_2$** complex in solution results in precipitation of the x(gas)@**Me,H,SiMe$_2$** ($x \leq 1$) clathrate, as gas-occupied forms of the 0D porous **Me,H,SiMe$_2$** phase. Interestingly, the occupancies of the CH_3Cl and CH_3Br clathrates, isolated under the same conditions, are nearly identical, despite the higher solubility of CH_3Br, suggesting that CH_3Cl is favored over CH_3Br. Similarly, the relatively high occupancy of the CH_3F (Freon-41) clathrate, despite the lower solubility of the gas, suggests that **Me,H,SiMe$_2$** exhibits a similar affinity for Freon-41 as CH_3Cl. Also, from a structural perspective, CH_3F demands the least perturbation of the **Me,H,SiMe$_2$** host structure (τ, V_{cell}, V_{cav}), relative to the empty form, in order to accommodate to the gas. Thus, it appears that the 0D porous phase of **Me,H,SiMe$_2$** exhibits affinity for methylhalides that follows the order $CH_3Cl > \approx CH_3F > CH_3Br$.

When **Me,H,SiMe$_2$** solutions were similarly treated with 1 atm of nonpolar, more weakly interacting gases such as ethane, ethylene, carbon dioxide, dimethyl ether, noble gases, and nitrogen, no gas clathrates formed, reflecting both the lower solubility of these gases and the lower binding constant of **Me,H,SiMe$_2$** toward these gases. Nonetheless, clathrates of each of these gases could be obtained as single crystals (no attempts were made to grow single crystals of the acetylene clathrate), and their structures determined, simply by pressurizing dry, saturated solutions ($CHCl_3$ or EtOAc) of **Me,H,SiMe$_2$** with the gas of interest.

Certain gases required only low overpressures to generate significantly occupied x(gas)@**Me,H,SiMe$_2$** ($x \leq 1$) clathrates. For example, single crystals of $0.82(CH_3OCH_3)$@**Me,H,SiMe$_2$** and (CH_3CH_2Cl)@**Me,H,SiMe$_2$** were obtained at pressures less than a few bar. Similarly, relatively low pressures of xenon, krypton, and C_2 gases gave significantly occupied crystals. Other, less soluble and/or more weakly interacting gases (CO_2, N_2), however, required high pressures to obtain even moderate occupancy crystals. The preparation of these gas clathrates required rigorous exclusion of water in order to avoid formation of mixed x(gas)/$y(H_2O)$@**Me,H,SiMe$_2$** compositions. Thus, under well-defined gas pressures, crystals of the following x(gas)@**Me,H,SiMe$_2$** clathrates were grown and their structures were determined at 100 K: $x = 0.34(2)N_2$ (80 bar N_2), $0.61(4)$Ar (80 bar Ar), $0.79(6)CH_4$ (36 bar CH_4), $0.42(1)CO_2$ (25 bar CO_2), $0.50(4)$Kr (9.8 bar Kr), $0.79(2)$Xe (9.8 bar Xe), $0.61(4)C_2H_4$ (9.8 bar C_2H_4), and $0.58(1)C_2H_6$ (9.8 bar C_2H_6), the occupancies being estimated by SCXRD. Several additional samples grown under elevated, but unmeasured, pressures were also prepared and analyzed by SCXRD (Table 1), including x(gas) = $0.51(3)$Kr, $0.77(3)$Xe, $0.72(2)C_2H_6$, and $0.46(6)CO_2$. Except for the precise occupancies of the gases, and effects related to the corresponding response of the crystal packing to the different occupancies, these structures are essentially identical to those with differing occupancies.

Several of the gas occupancy trends require comment as the selective enclathration of gases by **Me,H,SiMe$_2$** suggests opportunities to apply **Me,H,SiMe$_2$** toward the separation of gases. For example, the noncryogenic separation of xenon and krypton remains an important problem[42] and **Me,H,SiMe$_2$** enclathrates more xenon than krypton at similar gas overpressures. After accounting for the greater solubility of xenon, however, it appears that the noble gas selectivity is likely low. Indeed, the **Me,H,SiMe$_2$** cavity is too small for optimal xenon binding, even in its expanded form (V_{cav} = 66 Å^3). In related work, we have found that spheroidal cavities smaller than about 70 Å^3 are simply too small to bind xenon strongly.[12]

Among the most interesting selectivity trends is the ability of **Me,H,SiMe$_2$** to capture and retain small amounts of methane and highly volatile C_2 hydrocarbons (ethane, ethylene, acetylene) as compared to its complete exclusion of the less volatile C_3 hydrocarbons propane and propene. Indeed, we were unable to prepare **Me,H,SiMe$_2$** clathrates of propane or propene even under pressurized conditions, implying that selectivity is directly attributable to the small size and 0D nature of the cavity/pore. On the basis of surface area and polarizability, one might expect a greater dispersion interaction between the higher surface area propane/propene and **Me,H,SiMe$_2$** as compared to the C_2 hydrocarbons, but the former are apparently either (i) too large or inappropriately shaped to be accommodated by molecular cavity of the host in solution or (ii) excluded from the crystal during the process of crystal nucleation and growth, which is capable of placing further three-dimensional constraints on the open-ended host cavity if the complex is to pack in the low-energy, empty-like monoclinic arrangement.

When a series of nonlinear gases of nearly identical size and shape are compared, the x(guest)@**Me,H,SiMe$_2$** occupancies follow the trend: chloroethane > dimethyl ether ≫ propane, propene (completely excluded). These occupancies can be understood on the basis of host−guest dipole−dipole interactions. Apparently, bent small molecules such as chloroethane (and methylene chloride solvent) are bound by **Me,H,SiMe$_2$** because they offer a significant dipole to compensate for the conformational and/or crystal packing stresses (i.e., energetic penalty) associated with their incorporation into the expanded molecular cavity. The nonpolar propane/propene gases apparently do not offer sufficient enthalpic interactions to compensate for what would be a necessary perturbation of the **Me,H,SiMe$_2$** crystal packing or its molecular conformation.

Interestingly, relatively high pressures were required for even modest uptake of CO_2. For example, CO_2 has about the same solubility as xenon in chloroform,[51] yet much more xenon is enclathrated under 9.8 bar of pressure than CO_2 under 25 bar of pressure. The result is understandable based upon their relative electronic polarizabilities. Interestingly, however, **Me,H,SiMe$_2$**

DOI: 10.1021/jacs.5b11395
J. Am. Chem. Soc. 2016, 138, 4377−4392

also enclathrates krypton more effectively than CO_2, despite its lower solubility and lower polarizability. It appears the spheroidal 0D cavity/pore of **Me,H,SiMe$_2$** is better suited to the complementary spheroidal gases than nonpolar, linear ones.

CH$_3$CCH@Me,H,SiMe$_2$·2CHCl$_3$. It was found that treatment of saturated solutions of **Me,H,SiMe$_2$** with 1 bar of propyne gas gave single crystals of CH$_3$CCH@**Me,H,SiMe$_2$**·2CHCl$_3$, the composition, structure, and stability of which is quite different from the other gas clathrates of **Me,H,SiMe$_2$**. Importantly, the isolation of CH$_3$CCH@**Me,H,SiMe$_2$**·2CHCl$_3$ (Figure 2, S61) illustrates a key difference between the solution binding properties of the **Me,H,SiMe$_2$** *molecule* and the gas affinity of the 0D porous **Me,H,SiMe$_2$** *material*. The linear, polar, propyne molecule is somewhat strongly bound by **Me,H,SiMe$_2$** in CHCl$_3$ solution. It is simply too long, however, to be accommodated within the 0D pores of the empty-like, *C*2/*c* crystal phase of the **Me,H,SiMe$_2$**. The solution-formed CH$_3$CCH@**Me,H,SiMe$_2$** complexes must therefore adopt a different packing arrangement in the solid state; the resulting arrangement leaves room for the inclusion of two molecules of solvent, forming CH$_3$CCH@**Me,H,SiMe$_2$**·2CHCl$_3$. A minor consequence of this fact is that the methyl group of the propyne molecule is not found to penetrate the cavitand cavity as deeply (d = 0.52 Å) as the longer guests that are trapped within the empty-like 1:1 phase (e.g., CH$_3$I@**Me,H,SiMe$_2$**, d = 0.30 Å, *vide infra*). A much more important consequence concerns the kinetic stability of the resulting gas clathrate. Whereas the gas-loaded clathrates of the 0D porous x(gas)@**Me,H,SiMe$_2$** ($x \leq 1$) phase are unusually stable, kinetically confining light gases at room temperature (*vide infra*), crystals of CH$_3$CCH@**Me,H,SiMe$_2$**·2CHCl$_3$ decompose relatively rapidly. In fact, unlike the clathrates of the 0D porous **Me,H,SiMe$_2$** phase, all propyne appears to be lost after light grinding of the sample in preparation for TGA analysis, presumably concomitant with solvent loss. Similarly, unlike the gas clathrates of much more volatile, but smaller gases (e.g., C$_2$H$_6$@**Me,H,SiMe$_2$**), no propyne remains in the powdered samples after 7 days of storage under ambient conditions. Therefore, it is clear that, while **Me,H,SiMe$_2$** can bind a variety of molecules *in solution*, the *confinement* and *sorptive* properties of the **Me,H,SiMe$_2$** *material* are highly dependent upon the crystal structure of the clathrates.

Notably, also, CH$_3$CCH@**Me,H,SiMe$_2$**·2CHCl$_3$ is, to our knowledge, the first crystal structure determination of the propyne molecule that is not coordinated to a metal. Moreover, the fact that the methyl group of the CH$_3$CCH (vs the alkynyl ≡C−H) is found to be buried in the cavity, with no apparent positional disorder, is an interesting observation. From $\Delta\delta$ effects, Cram and co-workers had suggested that CH$_3$CCH resides with the alkynyl moiety pointing into the cavity in the solution complex of CH$_3$CCH@**H,Me,SiMe$_2$**.[39c]

3.2.3. Semiflexible 0D Pores: Structural Consequences of Gas Accommodation. Understanding framework flexibility in porous materials is becoming increasingly important, particularly as it relates to gas transport/diffusion in molecule-derived porous materials.[52−54] In this sense, the numerous single crystal structure determinations of x(gas/guest)@**Me,H,SiMe$_2$** ($x \leq 1$) clathrates constitute an unusual example of a systematic, sub-angstrom resolution exploration of the structural characteristics of small, semiflexible nanospaces and their response to molecular probes. These data shed light on the structure−selectivity and structure−stability relationships in **Me,H,SiMe$_2$** that are certain to be relevant to other 0D porous solids. Moreover, the existence of kinetically stable gas clathrates of **Me,H,SiMe$_2$** also provides a means to study the structure and properties of gas molecules in a highly confined, crystalline environment. Though the amount of available information from these structure determinations is too vast to describe in detail, some telling structural features are apparent and will be highlighted here.

First, several of the reported clathrates are unusual with respect to the confined gas. For instance, 0.80(4)CH$_3$F@**Me,H,SiMe$_2$** constitutes only the second crystal structure determination of the volatile fluoromethane molecule (Freon 41, bp = −78 °C), our recent report of 0.69(CH$_3$F)@**Me,Et,SiMe$_2$** being the first.[9] Due to rather extensive variation in bond lengths involving fluorine, the covalent radius of fluorine has been the subject of considerable discussion. The C−F bond length, for example, varies from ∼1.32 to ∼1.39 in the series of fluoromethanes. The C−F bond length in 0.80(4)CH$_3$F@**Me,H,SiMe$_2$** measures 1.391(4) Å, in excellent agreement with the spectroscopic value of 1.391(5) Å, the value of 1.389 Å calculated at the MP2/6-311+G** level,[55,56] and the previously determined value of 1.389(3) Å in 0.69(CH$_3$F)@**Me,Et,SiMe$_2$**. Similarly, 0.88(CH$_3$SH)@**Me,H,SiMe$_2$** appears to be the first instance of methyl mercaptan (noncoordinated) in the CSD. Similarly, the CSD contains only one atomic-resolution structure containing an ordered, noncoordinated ethylene molecule—pure ethylene at 85 K[57]—and only two examples of ordered ethane—that from a twinned ethane crystal at 85 K[58] and a twinned crystal of the C$_2$H$_6$@C$_{60}$ clathrate, another 0D porous clathrate.[36] Moreover, the crystallographic characterization of chloromethane[59] and chloroethane[60] has only recently been reported, and under high pressure conditions. Ordered structures of noncoordinated dinitrogen complexes are also rare.

The enclathrated gases experience some interesting trends in terms of their degree of thermal motion. Smaller, less polar, and lighter gases enclathrated by **Me,H,SiMe$_2$** (e.g., CO_2, CH$_3$CH$_3$, H$_2$C═CH$_2$, CH$_3$F) clearly exhibit a greater degree of thermal motion at 100 K than do the larger, more polar, and heavier molecules bound in the x(guest)@**Me,H,SiMe$_2$** phase. For instance, while CH$_3$F exhibits larger thermal parameters than the larger and heavier CH$_3$Cl, CH$_3$F is clearly more fixed by the **Me,H,SiMe$_2$** cavity at 100 K than the larger, similar mass ethane molecule, or the heavier CO_2 molecule. The effect is likely a manifestation of enthalpy−entropy interplay in these supramolecular systems. Regardless, each of these volatile gases is found to be generally ordered within the cavity at 100 K and can be refined without restraints. For instance, the freely refined ethane C−C bond and ethylene C═C bond lengths in 0.72(2)CH$_3$CH$_3$@**Me,H,SiMe$_2$** and 0.41(4)C$_2$H$_4$@**Me,H,SiMe$_2$** are 1.500(6) Å and 1.334(9) Å, respectively, as compared to the accepted values of 1.54(2) Å[58] and 1.336(3) Å,[57] respectively. The value for ethane suggests that it may be artificially short due to effects of libration. Similarly, the freely refined N≡N bond in 0.34(1)N$_2$@**Me,H,SiMe$_2$** (0.918(12) Å) appears to be artificially short.

The series of methyl-terminated and rare gas clathrates also show some telling trends in terms of the positioning of the guests within the cavity. For each series, the unit cells, cavity volumes, and $\Delta\tau$(avg) values scale with the volume of the enclathrated guest molecules. Like the partial hydrates, the V_{cell} of the CH$_3$F, Ar, and even Kr clathrates are more-or-less indistinguishable from empty **Me,H,SiMe$_2$** whereas larger guests induce a greater degree of cavity and unit cell expansion (larger $\Delta\tau$(avg) and larger V_{cell}). As expected, the positioning of rare gases within the **Me,H,SiMe$_2$** cavity follows their atomic radii. That is, the depth of penetration of the rare gas atom within the cavity can be

DOI: 10.1021/jacs.5b11395
J. Am. Chem. Soc. 2016, 138, 4377−4392

quantified by its distance, d, above the plane of upper-rim arene ring carbon atoms, with argon (d = 0.32 Å) residing deeper in the cavity than krypton (d = 0.42 Å), residing deeper than xenon (d = 0.59 Å). Thus, even at low gas occupancy, krypton and xenon can easily be distinguished from argon (or water, d = 0.29(4) Å) simply based on their position in the cavity.

Similarly, within the methylhalide series, the depth of penetration of the methyl group, and the tilt angle, ϕ, of the linear guest relative to the normal of the plane of the upper rim aryl carbon atoms follows the order CH_3F (d = 0.59 Å, ϕ = 4.1°) < CH_3Cl (d = 0.45 Å, ϕ = 11.5°) < CH_3Br (d = 0.38 Å, ϕ = 16.4°) < CH_3I (d = 0.30 Å, ϕ = 28.6°). Acetonitrile, of smaller volume but nearly identical length to CH_3I, is similarly compressed into the cavity of CH_3CN@**Me,H,SiMe$_2$** (d = 0.32 Å, ϕ = 8.4°), though C−H···N close contacts involving the neighboring **Me,H,SiMe$_2$** molecule near the upper rim of the cavity appear to allow CH_3CN to maintain a greater degree of linearity with respect to the C_4 axis of the host. From this series, it is clear that the **Me,H,SiMe$_2$** host mitigates potential protrusion (and crystal expansion) of increasingly longer guests from the upper rim of the host cavity by forcing the linear guests to tilt along their long axis and, additionally, by pushing the methyl group deeper into the cavity, by up to 0.3 Å. Apparently, the energetic penalty of tilting these guests is offset by the maintenance of otherwise more optimal host−host intermolecular contacts throughout the rest of the crystal. Importantly, however, the stress of accommodating the larger gases has consequences for the thermodynamic and kinetic stability of these clathrates (*vide infra*). This conclusion is consistent with the clathrate structures of the largest gases, namely CH_3CH_2Cl@**Me,H,SiMe$_2$** and 0.82(4)CH_3OCH_3@**Me,H,SiMe$_2$**, wherein the guests are forced to penetrate more deeply (d = 0.28 and 0.36 Å, respectively) and pack more densely within the maximized cavity volume (see PF_{cav}, Table 1), as opposed to inducing an even greater volume expansion of the host structure. The conclusion is also supported by the structure of the aforementioned CH_3CCH@**Me,H,SiMe$_2$**·2$CHCl_3$. Residing within cavitands that adopt a different packing motif, the propyne molecule does not suffer from guest compression (d = 0.52 Å). Propyne is simply too long to be accommodated by the 0D pore offered by **Me,H,SiMe$_2$** and thereby induces an alternative packing mode during crystallization, one which provides little kinetic stability.

Lastly, it was observed that, despite offering essentially the same *molecular* cavity, CO_2 molecules in the previously reported 0.20CO_2@**Me,Et,SiMe$_2$** clathrate are situated in the cavity somewhat differently than the CO_2 molecules in the $x$$CO_2$@**Me,H,SiMe$_2$** clathrates reported here (Scheme 2). In 0.20CO_2@**Me,Et,SiMe$_2$**, the CO_2 molecule resides deeper in the cavitand, by Δd = 0.15 Å, and is far more tilted relative to the psedo-C_4 axis of the cavitand (ϕ = 57° vs 38°); it also exhibits much shorter (CO_2)O···Si (3.62 vs 4.19 Å) intermolecular contacts, near the sum of the van der Waals radii. It appears the intrinsic pore offered by the **Me,Et,SiMe$_2$** packing is effectively smaller than in **Me,H,SiMe$_2$**. Indeed, the ethyl groups of adjacent cavitands lie much nearer the upper rim of the cavitand in the crystal packing of **Me,Et,SiMe$_2$** than do the closest positioned groups in **Me,H,SiMe$_2$**. Thus, the orientation of the CO_2 molecule in the $SiMe_2$-bridged cavitands, and likely the material's affinity for CO_2, is affected by the crystal packing. Such effects would be absent for CO_2 binding in solution, highlighting another important difference between the thermodynamics of sorption in cavitand *materials* and the solution thermodynamics of binding by cavitand *molecules* in solution. Interestingly, also, gases generally appear to be better confined, kinetically, by **Me,H,SiMe$_2$** than **Me,Et,SiMe$_2$**, despite the effectively smaller cavities in the latter. We speculate that the stability difference is related to the presence of potentially dynamic ethyl groups in the **Me,Et,SiMe$_2$** compound, which may facilitate gas permeation.

4. Kinetic Confinement of Gases. *4.1. Single-Crystal-to-Single-Crystal (SC → SC) Activation.* Like crystals of x(H_2O)@**Me,Et,SiMe$_2$**,[9] the partial hydrate crystals of **Me,H,SiMe$_2$** can be activated (emptied, dehydrated) in a SC → SC fashion by placing them in an oven at 150 °C for about a day. Thus, a single crystal of 0.21(2)H_2O@**Me,H,SiMe$_2$** (1.6 × 1.5 × 0.96 mm^3), obtained by slow evaporation of **Me,H,SiMe$_2$** from a chloroform solution, was dehydrated at 150 °C, after which a second data collection (100 K) was performed on the crystal. The electron density attributed to water in the first collection was clearly absent in the second and the largest residual peak in the difference Fourier map (0.25 e$^-$/Å^3) was significantly offset from the center of the cavity, demonstrating that the cavities are empty. The empty single crystal of **Me,H,SiMe$_2$** (1.6 × 1.5 × 0.96 mm^3) could also be partially rehydrated. After residing in a 100% relative humidity chamber at room temperature for approximately 3 weeks, a third data collection (100 K) revealed that the pore had taken up, on average, approximately 0.29(2) equiv of water as estimated by SQUEEZE analysis and refinement of the occupancy of the water oxygen atom. Clearly, like the reported **Me,Et,SiMe$_2$**, **Me,H,SiMe$_2$** is permeable to water.

The x(gas)@**Me,H,SiMe$_2$** ($x \leq 1$) clathrates generally exhibit a remarkable kinetic stability. In general, for most clathrates, heating (commonly above 100 °C) is required to remove the guests (gases or solvents) from the material at a reasonable rate. For example, despite the low normal boiling points of many of the gaseous guests, the isolated x(gas)@**Me,H,SiMe$_2$** crystals do not require any special handling and show no sign of gas loss at room temperature on a time scale of hours to months, depending upon the identity of the confined gas. This confinement property is no doubt a relatively extreme manifestation of the "closed pore" or microcavity structure of the clathrates, the behavior being akin to the van der Waals confinement properties of calix[4]arene·$x$gas,[30] C_{60}·gas,[36] and hydroquinone·$x$gas[61] extrinsic clathrates and the recently reported Xe@(±)-cryptophane-111 intrinsic gas clathrate.[12]

As a probe of their stability, the original x(gas)@**Me,H,SiMe$_2$** clathrate single crystals of some of the most volatile guests that were analyzed by SCXRD—x(gas) = 0.29(2)Ar, 0.77(3)Xe, 0.41(4)C_2H_4, 0.72(2)C_2H_6, 0.46(6)CO_2—were kept in a desiccator at room temperature and again analyzed by single crystal X-ray diffraction, after 7, 112, 7, 10, 10 days, respectively. Similarly, a different crystal of x(CH_3F)@**Me,H,SiMe$_2$**, selected from the same original batch preparation of 0.80(4)CH_3F@**Me,H,SiMe$_2$** was analyzed after 146 days at ambient conditions. Likewise, a different crystal of $x$$N_2$@**Me,H,SiMe$_2$**, selected from the same original batch preparation of 0.34(1)N_2@**Me,H,SiMe$_2$**, was analyzed after 54 h at room temperature (desiccator). Notably, none of the crystals lost their transparency or showed significantly diminished diffraction intensities over this time frame. With the exception of the x(CH_3F)@**Me,H,SiMe$_2$**, x(CO_2)@**Me,H,SiMe$_2$**, and x(N_2)@**Me,H,SiMe$_2$** crystals, the occupancies of the other x(gas)@**Me,H,SiMe$_2$** single crystals were identical to the original measurement within the estimated precision of the measurement (ca. ± 3%). That is, argon, xenon, ethylene, and ethane—with normal boiling points of −186, −108, −104, and −89 °C, respectively—are kinetically confined

DOI: 10.1021/jacs.5b11395
J. Am. Chem. Soc. 2016, 138, 4377−4392

within submillimeter sized single crystals for periods of at least several days to months (xenon).

After 146 days at room temperature, a $x(CH_3F)$@**Me,H,SiMe$_2$** crystal, selected from a batch prepartion of $0.80(4)CH_3F$@**Me,H,SiMe$_2$**, gave a refined occupancy of $x \approx 0.45(11)$, though there was a strong indication from the data—artificial elongation of the C−F bond, greater than expected electron density at the carbon position relative to the fluorine position—that the $x(CH_3F)$@**Me,H,SiMe$_2$** crystal had taken up a small amount of atmospheric water vapor during this time. In fact, the 146 day old crystal could be refined, more satisfactorily, as $0.37(CH_3F),0.14(H_2O)$@**Me,H,SiMe$_2$**. The crystal was then heated at 150 °C for 4 days; redetermination of the structure of this crystal gave a refined occupancy of $x = 0.23(1)$ for the CH_3F molecule. That is, incredibly, 146 days at room temperature, followed by storage of the crystal for 4 days at temperatures greater than 225 °C above the normal boiling point of the gas, was insufficient to completely degas the crystal. Further heating of the $0.23(1)CH_3F$@**Me,H,SiMe$_2$** crystal for 4 days at 190 °C finally emptied it entirely, in a SC → SC fashion. The crystal suffered no meaningful loss in diffracting power over the course of these treatments. Of course, the greater kinetic stability of the CH_3F clathrate vs the aforementioned H_2O clathrate can be attributed to the larger size of Freon-41 and the greater thermodynamic affinity of the cavitand for this guest.

The gases being much smaller, single crystals of $x(N_2)$@**Me,H,SiMe$_2$** and $x(CO_2)$@**Me,H,SiMe$_2$** lose their gases over a period of days at room temperature. Single crystals of the nitrogen clathrate of **Me,H,SiMe$_2$** were grown under 80 bar of nitrogen. One was analyzed by SCXRD, giving an occupancy of $x = 0.34(1)N_2$. A second, higher quality, crystal of $x(N_2)$@**Me,H,SiMe$_2$** selected from the same batch sample was analyzed, but after the crystals had been stored at room temperature, in a desiccator, for 54 h. The second crystal gave a refined occupancy of $0.23(2)N_2$@**Me,H,SiMe$_2$**, likely due to partial N_2 loss during storage. The N_2 bond length in this crystal was refined to be 0.923(15) Å, somewhat consistent with the first structure determination, and artificially short due to libration effects. Immediately following the low temperature data collection, the second crystal was returned to the desiccator and stored at room temperature for another 179 h (9 days, 17 h in total at room temperature), after which another data collection was obtained. The composition of the crystal at this time was refined to be $0.14(5)N_2$@**Me,H,SiMe$_2$**; the N_2 was refined with isotropic displacement parameters, and the bond length was freely refined to a value of 0.98(3) Å. Notably, the crystal showed no deterioration in diffraction quality upon N_2 loss.

After 10 days at room temperature, the original single crystal of $0.46(6)CO_2$@**Me,H,SiMe$_2$** gave a refined composition of $0.35(5)CO_2$@**Me,H,SiMe$_2$**. Thus, it appears that **Me,H,SiMe$_2$** is more permeable to N_2 and CO_2 (higher diffusion coefficients) than to other, larger gases, almost certainly likely due to the smaller kinetic diameters of N_2 and CO_2 (3.64 and 3.30 Å, respectively) and the lesser thermodynamic affinity of the cavitand for these gases. That xN_2@**Me,H,SiMe$_2$** appears to degas faster than xCO_2@**Me,H,SiMe$_2$**, despite CO_2 having a smaller kinetic diameter, is likely due to the greater enthalpic stability of the CO_2@**Me,H,SiMe$_2$** complex.

Clearly, the kinetics of guest loss are highly guest dependent. The original single crystal of 0.54(3)Kr@**Me,H,SiMe$_2$** was reexamined by SCXRD after 10 days in the oven at 100 °C. The composition was determined to be 0.07(1)Kr@**Me,H,SiMe$_2$**. Notably, the crystal showed almost no deterioration in diffraction quality upon Kr loss, as evidenced by the percent of observed reflection intensities (69% and 67% to $2\theta = 50°$ for 0.54(3)Kr@**Me,H,SiMe$_2$** and 0.07(1)Kr@**Me,H,SiMe$_2$**, respectively). The magnitude of the electron density (>0.5 oxygen) and its position (d = 0.43 Å) in the cavity, however, allows the unambiguous conclusion that the electron density found with the cavitand cavities after heating of the crystal corresponds to residual krypton, as opposed to other conceivable assignments (e.g., a water molecule: where the maximum observed occupancy is about 0.38 eq., and $d = 0.30(2)$ Å).

In general, it was found that, if the unit cell volumes of the crystal do not appreciably contract upon emptying, single crystals of the x(gas)@**Me,H,SiMe$_2$** clathrates could be readily degassed while preserving single crystallinity. Single crystal clathrates of the larger volume guests (e.g., CH_2Cl_2, Xe, even CH_3Cl), however, tended to fracture under the stress of thermally induced degassing, presumably due to nonuniform crystal contraction.

4.2. Thermal Gravimetric Analyses (TGA). TGA of the bulk x(gas)@**Me,H,SiMe$_2$** samples further underscores the kinetic stability of the x(gas)@**Me,H,SiMe$_2$** clathrates. Figure 4 shows,

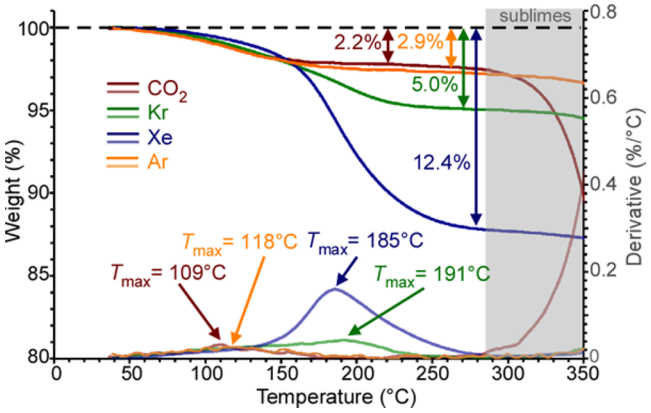

Figure 4. TGA of selected x(gas)@**Me,H,SiMe$_2$** ($x \leq 1$) clathrates, highlighting their general and relative kinetic stabilities. The maximum of the derivative mass loss curves is defined as T_{max}. $T_{max} - T_{bp}$ (315 °C, Ar; 334 °C, Kr; 293 °C, Xe; 187 °C, CO_2) may be considered a semiquantitative measure of the relative degree of gas confinement. The mass losses observed by TGA agree well with the expected values based upon SCXRD occupancies (Table 1).

for example, the TGA curves of four selected clathrates; the remaining TGA analyses are provided as SI. The TGA data also serve, in many samples, to validate the gas occupancies obtained by refinement of the SCXRD data. The onset temperatures for gas loss are difficult to define due to the very slow initial release rates below 100 °C, though we have found that the T_{max} values (Table 1)—the temperature that defines the maximum rate of mass loss for a standard heating rate (5 °C/min)—are fairly reproducible (±5 °C) for finely powdered samples and serve as a practical indicator of the relative kinetic stability of the clathrates. Moreover, the parameter $T_{max} - T_{bp}$ (Table 1), where T_{bp} is the normal boiling point of the gas, can be considered a useful semiquantitative indicator of the extent to which a material is capable of kinetically confining an otherwise volatile gas.

Notably, for several clathrates, TGA analysis in open TGA pans led to artificially high weight loss (as compared to SCXRD and ^{1}H NMR, where applicable); we surmise this is due to cosublimation of **Me,H,SiMe$_2$** induced by gas loss. For such samples, TGAs were carried out by placing the powdered samples in a sealed DSC pan (see SI), with pinholes that allow

DOI: 10.1021/jacs.5b11395
J. Am. Chem. Soc. 2016, 138, 4377−4392

gas escape. For many gas clathrarates (e.g., those of Ar, CH_4, Kr, Xe, C_2H_4, C_2H_6, CH_3F), this technique gave mass losses that were much more reproducible and consistent with ^{1}H NMR and/or SCXRD analyses. Several gas clathrates were also characterized by tandem TGA mass spectrometry (TGA-MS), allowing confirmation of the identity of the evolved gas species.

According to their T_{max} values, the relative kinetic stability of the gas clathrates in Figure 4 follows the order: CO_2 < Ar < Kr ≈ Xe. Though the T_{max} values of this series correlate with the kinetic diameters of these gases, the kinetic diameter of a gas is not the only factor that governs the kinetic stability of the clathrates. Importantly, the kinetics of desorption are also influenced by the thermodynamic stability of the guest@**Me,H,SiMe$_2$** clathrates and the crystal packing. These factors are clearly observed in the behavior of the methylhalide clathrates. For example, the T_{max} values of 0.80(4)CH_3F@**Me,H,SiMe$_2$** and CH_3I@**Me,H,SiMe$_2$** are about the same (T_{max} = 203-210 °C), despite the very different kinetic diameters and boiling points of these guests. And both the chloromethane and bromomethane clathrates are slightly more stable (T_{max} ≈ 230 °C). We suggest that iodomethane is relatively poorly confined, in spite of its relatively large kinetic diameter, because of the fact that the CH_3I@**Me,H,SiMe$_2$** (V_{cell} = 8371 Å^3) structure is somewhat expanded relative to empty **Me,H,SiMe$_2$** (V_{cell} = 8230 Å^3). The expansion of host packing that must occur in order to accommodate CH_3I comes at a cost in terms of the thermodynamic stability of the CH_3I@**Me,H,SiMe$_2$** complex in the solid state. Another consideration is that the expanded host structure likely has effectively larger transient pores, through which the guest may escape more easily. Similarly, the $x$$CH_2Cl_2$@**Me,H,SiMe$_2$** ($T_{max}$ ≈ 180 °C) clathrate is significantly less stable than $x$$CH_3F$@**Me,H,SiMe$_2$** ($T_{max}$ ≈ 200 °C) despite the large kinetic diameter of CH_2Cl_2 and its much higher boiling point. Clearly, the kinetic stability of $x$$CH_2Cl_2$@**Me,H,SiMe$_2$** is compromised by its relatively low thermodynamic stability, due to the poor complementarity/fit between the relatively large solvent and the tiny cavity/pore. Likewise, the $x$$CH_3CH_2Cl$@**Me,H,SiMe$_2$** clathrate is even less kinetically stable (T_{max} = 158 °C), due its relatively low thermodynamic stability. The high packing fraction of these guests within the cavity (PF_{cav} = 0.80) also underscores the strain of the expanded host structure, attributable to the built-in stresses of these clathrates.

Thus, in general, it appears that, if the guest is of a size that is complementary to the empty 0D pore and the resulting guest@**Me,H,SiMe$_2$** clathrates are not appreciably expanded relative to empty **Me,H,SiMe$_2$**, the kinetic stability of the clathrates correlates well with the kinetic diameter of the guest and the thermodynamic affinity of the host for the guest. The kinetic stability of the clathrate is appreciably compromised; however, if the guest is effectively too large for the cavity, the result, interestingly, is that certain volatile gases may be confined by **Me,H,SiMe$_2$** to temperatures far exceeding their normal boiling points (e.g., $T_{max} - T_{bp}$ > 300 °C for Ar, Kr, CH_3F) whereas some higher boiling guests (e.g., CH_2Cl_2), generally more capable of stronger intermolecular interactions, are less confined by **Me,H,SiMe$_2$**, especially relative to their normal boiling points. We believe these factors affecting kinetic stability can be generalized to other clathrates of 0D porous materials.

4.3. Surface Area and Pore Volume. The relatively high gas desorption temperatures for x(gas)@**Me,H,SiMe$_2$** clathrates arise from large kinetic barriers to gas egress due to the absence of windows—even transient ones, due to the inflexibility of the molecule—connecting the 0D pores in **Me,H,SiMe$_2$**. The barrier to ingress is of course similarly large. Indeed, single crystals of empty **Me,H,SiMe$_2$** do not appear to absorb most gases at an appreciable rate, even at room temperature at elevated pressures. Thus, **Me,H,SiMe$_2$** is not a candidate for the determination of internal surface area or pore volume by traditional gas sorption isotherm measurements, which are performed at low temperatures and low pressures and only provide data on pores that are accessible under these conditions. Nonetheless, the crystal structures allow quantification of not only the idealized internal volume of **Me,H,SiMe$_2$** (29 cm^3(STP)·g^{-1}, for an ideal gas) but also the hypothetical surface area. Depending upon the sorbate considered—e.g., Ar, CO_2, with areal diameters of 13.8 and 19.5 Å^2, respectively—one arrives at a specific surface area of 108–153 m^2/g for **Me,H,SiMe$_2$**, allowing for a total capacity of one molecule per cavity. In all cases, the cavity is too small to accommodate more than one molecule, at most, of the gases studied.

4.4. Gas/Vapor Sorption Kinetics Monitored by SCXRD. 4.4.1. Water Vapor Sorption Kinetics. Since water has one of the smallest kinetic diameters (2.6 Å) and a reasonably high equilibrium occupancy in **Me,H,SiMe$_2$** at room temperature and high humidity, we sought to monitor the *kinetics* of water vapor sorption **Me,H,SiMe$_2$**. A single crystal (1.25 × 1.18 × 0.66 mm^3) of empty **Me,H,SiMe$_2$** was placed in a chamber at 100% relative humidity at room temperature (P_{H_2O} ≈ 2.8(3) bar) and the water occupancy of the crystal was estimated periodically by low temperature SCXRD (100 K, thereby temporarily halting the sorption process during analysis) over a period of several weeks (Figure 5, Table S2). The occupancy of refined oxygen atom

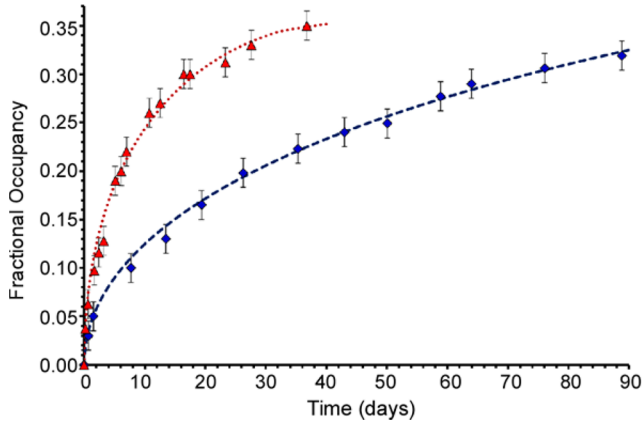

Figure 5. Kinetics of water vapor (red) (P_{H2O} = 0.028(3) bar, estimated; 1.25 × 1.18 × 0.66 mm^3 crystal) and CO_2 sorption (blue) (P_{CO2} = 25.0(2) bar; 0.57 × 0.55 × 0.40 mm^3 crystal) at room temperature by 0D porous **Me,H,SiMe$_2$** as measured by SCXRD. The data are plotted as the freely refined average fractional occupancy vs time (days) with estimated standard errors of ±1.5%. Dashed and dotted lines represent the best fit to the Ginstling–Brounshtein (D4, eq 1) diffusion model (see SI).

position and the total electron density found within the pore exhibited a continuous increase with time. Only after more than 37 days under these conditions did the single crystal reach the near-equilibrium composition of approximately 0.35(2)H_2O@**Me,H,SiMe$_2$**, highlighting the extremely slow, diffusion controlled uptake of water vapor by **Me,H,SiMe$_2$**. The data were analytically fit to different deceleratory kinetic models (D1, D2, D3, D4, F1, *etc.*). Despite the nonspherical shape of the single

DOI: 10.1021/jacs.5b11395
J. Am. Chem. Soc. 2016, 138, 4377–4392

crystal, the data were well fit (R^2 = 0.9957) to the Ginstling–Brounshtein (D4) 3D spherical diffusion model (eq 1; k is the rate constant (h^{-1}), α = fractional conversion to the equilibrium occupancy, t = time).[62] The fit yielded a rate constant, k, of $3.45(13) \times 10^{-4}$ h^{-1} and an equilibrium crystal composition of $0.352(2)H_2O$@**Me,H,SiMe$_2$** (see SI). The D4 diffusion model appears to suggest that water diffusion through **Me,H,SiMe$_2$** is not limited to one specific path or tunnel.

$$1 - 2\alpha/3 - (1 - \alpha)^{2/3} = kt \quad (1)$$

4.4.2. CO_2 Sorption Kinetics. The kinetic diameter of CO_2 (3.3 Å) is larger than water, but it is nonetheless sufficiently small that its sorption by **Me,H,SiMe$_2$** can be followed over time and monitored by SCXRD. An empty single crystal of **Me,H,SiMe$_2$** ($0.57 \times 0.55 \times 0.40$ mm^3, more uniformly shaped than that employed for monitoring water sorption) was placed in a customized stainless steel vessel, in the presence of 3 Å molecular sieves, and pressurized with 25 bar of carbon dioxide. The crystal was removed periodically from the pressurized vessel for structure determination at 100 K by SCXRD. The crystal was then immediately returned to pressurized conditions following data collection. Control experiments demonstrated that, during the required room temperature manipulations, there was no observable change in the overall CO_2 occupancy, nor does the crystal measureably absorb air gases. Moreover, there is no measurable rate of sorption of N_2 by crystals of **Me,H,SiMe$_2$** at low temperature. Thus, in this way, the average CO_2 content of the pressurized crystal was estimated over 90 days by free refinement of the CO_2 occupancy parameter (Figure 5, Table S3). Thermal ellipsoid plots (50% probability level) for each $x(CO_2)$@**Me,H,SiMe$_2$** structure determination are given in Figure S4 and are fully consistent with the structure determinations of $x(CO_2)$@**Me,H,SiMe$_2$** crystals grown from solution under the pressure of CO_2. Remarkably, even after 90 days, the crystal had not yet reached equilibrium with respect to CO_2 uptake. As with sorption of water vapor, the data were best fit to a D4 diffusion model, allowing determination of the rate constant, $k = 3.32(97) \times 10^{-5}$ h^{-1}, and an estimation of the equilibrium composition of $0.49(6)CO_2$@**Me,H,SiMe$_2$**, corresponding to $\alpha = 1$.

As the kinetic data were acquired using different crystals, and different gas pressures, it is difficult to directly compare the rate of absorption of water with that of CO_2. That the crystal used to study water sorption was much larger, yet the rate of water sorption was much faster than CO_2, suggests, not surprisingly, that the kinetic diameters of the sorbates play an important role in governing sorption kinetics. These studies represent a rare, if not unprecedented, example of monitoring gas sorption *kinetics* by SCXRD. We believe that the relatively slow sorption kinetics of certain 0D porous materials such as **Me,H,SiMe$_2$** provide an unusual opportunity to study issues of diffusion and permeability in barrier solids and may shed light on a phenomenon that remains poorly understood in solid state chemistry.

CONCLUSIONS

The data presented here demonstrate that **Me,H,SiMe$_2$** exhibits highly unusual behavior with respect to gas enclathration and permeability, effectively confining all but the tiniest gases to high temperatures. These materials properties are governed by the intrinsically 0D porous crystal structure of the empty apohost, which appears to be the most thermodynamically stable structure of this compound. A key feature is the relatively nondynamic, incollapsible nature of the **Me,H,SiMe$_2$** cavitand, such that no significant change in host packing is necessary to permit accommodation of even weakly interacting light gases. Thus, akin to open pore materials, and despite its low overall porosity (ε = 2.7% in its empty form), **Me,H,SiMe$_2$** can readily accommodate complementary gases. The crystal structures of over 20 isostructural x(gas/guest)@**Me,H,SiMe$_2$** clathrates provide a detailed picture of the nature of sorbent–host interactions and sorbate accommodation, including the factors that influence the selective nature of guest/gas enclathration and kinetic confinement. The material can swell slightly ($\Delta V_{cell} < 3\%$, $\varepsilon \leq 7.7\%$) to accommodate larger guests/gases ($V_{guest} < 65$ Å^3), but only to a point, as expansion appears to destabilize the clathrates.

Importantly, the materials properties of **Me,H,SiMe$_2$** are not fully congruent with the well-known solution binding properties of related cavitands, as is evident by the properties of the propyne clathrate, CH_3CCH@**Me,H,SiMe$_2$**·$2CHCl_3$, which does not enjoy the same stability as the clathrates that are isostructural to the porous apohost phase. Similarly, the orientations of CO_2 molecules in xCO_2@**Me,H,SiMe$_2$** and the previously reported xCO_2@**Me,Et,SiMe$_2$** clathrate are different, illustrating that crystal packing significantly affects the pore properties. Structural analysis provides key insights into the remarkable stability of many x(gas)@**Me,H,SiMe$_2$** clathrates. Factors that appear to influence gas confinement ($T_{max} - T_{bp}$) are (i) the 0D/closed pore structure, (ii) the ordered, conformational rigidity of host, (iii) electronic and steric complementarity (thermodynamic affinity) between the gas and the pre-exisiting pore of the apohost, and (iv) the kinetic diameter of the gas.

Despite the ability of **Me,H,SiMe$_2$** to confine many gases, the material is formally permeable, albeit slightly. Single crystals of several x(guest)@**Me,H,SiMe$_2$** clathrates (guest = N_2, CO_2, Kr, CH_3F, H_2O) desorb their guests in a SC → SC fashion. For example, N_2 degasses over a period of days at room temperature whereas others require considerable heating. Moreover, single crystals of empty **Me,H,SiMe$_2$** have been demonstrated to absorb water vapor and CO_2 gas in a SC → SC fashion, despite there being no obvious dynamic mechanism to permit gas permeation. The data highlight the potential for **Me,H,SiMe$_2$**, and related 0D porous molecular solids, to be used as a sorbent under appropriate conditions. The mechanism of transport is not yet understood, but the sorption data fit well to a 3D deceleration model.

In conclusion, we have recently suggested that 0D porous structures are probably ubiquitous,[9] especially among shape-persistent, concave/macrocyclic compounds. It is now becoming clear that, from confinement properties to open-pore-like transient porosity, the properties of 0D porous materials merit further study.

ASSOCIATED CONTENT

Supporting Information

The Supporting Information is available free of charge on the ACS Publications website at DOI: 10.1021/jacs.5b11395.

Experimental procedures, TGA and ^{1}H NMR characterization, SCXRD summary data (including thermal ellipsoid plots), discussion on calculation of V_{cav} and PF_{cav}, guest occupancy (x) determination by SCXRD and TGA validation, SC → SC studies (PDF)

Crystallographic data (CIF)

Crystallographic data (CIF)

DOI: 10.1021/jacs.5b11395
J. Am. Chem. Soc. 2016, 138, 4377–4392

Crystallographic data (CIF)
Crystallographic data (CIF)
Crystallographic data (CIF)
Crystallographic data (CIF)
Crystallographic data (CIF)
Crystallographic data (CIF)
Crystallographic data (CIF)
Crystallographic data (CIF)
Crystallographic data (CIF)
Crystallographic data (CIF)
Crystallographic data (CIF)
Crystallographic data (CIF)
Crystallographic data (CIF)
Crystallographic data (CIF)
Crystallographic data (CIF)
Crystallographic data (CIF)
Crystallographic data (CIF)
Crystallographic data (CIF)
Crystallographic data (CIF)
Crystallographic data (CIF)
Crystallographic data (CIF)
Crystallographic data (CIF)
Crystallographic data (CIF)
Crystallographic data (CIF)
Crystallographic data (CIF)
Crystallographic data (CIF)
Crystallographic data (CIF)
Crystallographic data (CIF)
Crystallographic data (CIF)
Crystallographic data (CIF)
Crystallographic data (CIF)
Crystallographic data (CIF)
Crystallographic data (CIF)
Crystallographic data (CIF)
Crystallographic data (CIF)
Crystallographic data (CIF)
Crystallographic data (CIF)
Crystallographic data (CIF)

AUTHOR INFORMATION

Corresponding Author
*kth7@georgetown.edu

Notes
The authors declare no competing financial interest.

ACKNOWLEDGMENTS

This material is based in part upon work supported by the National Science Foundation (NSF) under Grant Number DMR-1106266. The work was also supported in part by NSF grants MRI-0959546 (equipment), CHE-1337975, and DMR-0843934 (C.M.K., International Research Fellowship, ICMR). C.M.K. acknowledges a Ludo Frevel Crystallography Scholarship from the International Center for Diffraction Data. We thank Dr. Ron Davis (Georgetown) for his assistance with TGA-MS and Dr. Vincent Smith (Stellenbosch) for help with some X-ray data collections.

REFERENCES

(1) Rudkevich, D. M. *Eur. J. Org. Chem.* **2007**, *2007*, 3255−3270.
(2) (a) Zhou, H.-C.; Kitagawa, S. *Chem. Soc. Rev.* **2014**, *43*, 5415. (b) *Metal-Organic Frameworks: Design and Application*; MacGillivray, L. R., Ed.; John Wiley & Sons: Hoboken, NJ, 2010. (c) Long, J. R.; Yaghi, O. M. *Chem. Soc. Rev.* **2009**, *38*, 1213−1214. (d) Ferey, G. *Chem. Soc. Rev.* **2008**, *37*, 191−214.
(3) (a) Côté, A. P.; Benin, A. I.; Ockwig, N. W.; O'Keeffe, M.; Matzger, A. J.; Yaghi, O. M. *Science* **2005**, *310*, 1166. (b) Feng, X.; Ding, X.; Jiang, D. *Chem. Soc. Rev.* **2012**, *41*, 6010.
(4) (a) McKeown, N. B.; Budd, P. M. *Chem. Soc. Rev.* **2006**, *35*, 675. (b) McKeown, N. B.; Budd, P. M. Polymers of Instrinsic Microporosity (PIMs). *Encyclopedia of Polymer Science and Technology*; John Wiley & Sons: Hoboken, NJ, 2010.
(5) (a) Mastalerz, M. *Chem. - Eur. J.* **2012**, *18*, 10082. (b) Holst, J. R.; Trewin, A.; Cooper, A. I. *Nat. Chem.* **2010**, *2*, 915.
(6) Dalgarno, S. J.; Thallapally, P. K.; Barbour, L. J.; Atwood, J. L. *Chem. Soc. Rev.* **2007**, *36*, 236. (b) Tian, J.; Thallapally, P. K.; McGrail, B. P. *CrystEngComm* **2012**, *14*, 1909.
(7) Huang, Z.; White, P. S.; Brookhart, M. *Nature* **2010**, *465*, 598.
(8) Little, M. A.; Briggs, M. E.; Jones, J. T. A.; Schmidtmann, M.; Hasell, T.; Chong, S. Y.; Jelfs, K. E.; Chen, N.; Cooper, A. I. *Nat. Chem.* **2015**, *7*, 153−159.
(9) Kane, C. M.; Ugono, O.; Barbour, L. J.; Holman, K. T. *Chem. Mater.* **2015**, *27*, 7337.
(10) (a) Thallapally, P. K.; Lloyd, G. O.; Atwood, J. L.; Barbour, L. J. *Angew. Chem., Int. Ed.* **2005**, *44*, 3848. (b) Dalgarno, S. J.; Tian, J.; Warren, J. E.; Clark, T. E.; Makha, M.; Raston, C. L.; Atwood, J. L. *Chem. Commun.* **2007**, 4848. (c) Erra, L.; Tedesco, C.; Cipolletti, V. R.; Annunziata, L.; Gaeta, C.; Brunelli, M.; Fitch, A. N.; Knöfel, C.; Llewellyn, P. L.; Atwood, J. L.; Neri, P. *Phys. Chem. Chem. Phys.* **2012**, *14*, 311. (d) Tsue, H.; Takahashi, H.; Ishibashi, K. *CrystEngComm* **2012**, *14*, 1021−1026.
(11) (a) Atwood, J. L.; Barbour, L. J.; Jerga, A.; Schottel, B. L. *Science* **2002**, *298*, 1000. (b) Atwood, J. L.; Barbour, L. J.; Thallapally, P. K.; Wirsig, T. B. *Chem. Commun.* **2005**, 51. (c) Atwood, J. L.; Barbour, L. J.; Jerga, A. *Angew. Chem., Int. Ed.* **2004**, *43*, 2948. (d) Thallapally, P. K.; Dobrzańska, L.; Gingrich, T. R.; Wirsig, T. B.; Barbour, L. J.; Atwood, J. L. *Angew. Chem., Int. Ed.* **2006**, *45*, 6506. (e) Thallapally, P. K.; Lloyd, G. O.; Wirsig, T. B.; Bredenkamp, M. W.; Atwood, J. L.; Barbour, L. J. *Chem. Commun.* **2005**, 5272. (f) Thallapally, P. K.; Wirsig, T. B.; Barbour, L. J.; Atwood, J. L. *Chem. Commun.* **2005**, 4420. (g) Thallapally, P. K.; McGrail, P. B.; Atwood, J. L. *Chem. Commun.* **2007**, 1521. (h) Ripmeester, J. A.; Enright, G. D.; Ratcliffe, C. I.; Udachin, K. A.; Moudrakovski, I. L. *Chem. Commun.* **2006**, 4986.
(12) (a) Joseph, A. I.; Lapidus, S. H.; Kane, C. M.; Holman, K. T. *Angew. Chem., Int. Ed.* **2015**, *54*, 1471. (b) Joseph, A. I.; El-Ayle, G.; Boutin, C.; Léonce, E.; Berthault, P.; Holman, K. T. *Chem. Commun.* **2014**, *50*, 15905.
(13) (a) Rudkevich, D. M.; Leontiev, A. V. *Aust. J. Chem.* **2004**, *57*, 713. (b) Leontiev, A. V.; Rudkevich, D. M. *Chem. Commun.* **2004**, 1468.
(14) (a) Yoon, M.; Suh, K.; Kim, H.; Kim, Y.; Selvapalam, N.; Kim, K. *Angew. Chem., Int. Ed.* **2011**, *50*, 7870. (b) Miyahara, Y.; Abe, K.; Inazu, T. *Angew. Chem., Int. Ed.* **2002**, *41*, 3020. (c) Lim, S.; Kim, H.; Selvapalam, N.; Kim, K.-J.; Cho, S. J.; Seo, G.; Kim, K. *Angew. Chem., Int. Ed.* **2008**, *47*, 3352. (d) Tian, J.; Ma, S.; Thallapally, P. K.; Fowler, D.; McGrail, P. B.; Atwood, J. L. *Chem. Commun.* **2011**, *47*, 7626. (e) Feng, X.; Chen, K.; Zhang, Y.-Q.; Xue, S.-F.; Zhu, Q.-J.; Tao, Z.; Day, A. I. *CrystEngComm* **2011**, *13*, 5049. (f) Kim, H.; Kim, Y.; Yoon, M.; Lim, S.; Park, S. M.; Seo, G.; Kim, K. *J. Am. Chem. Soc.* **2010**, *132*, 12200.
(15) (a) Eddaoudi, M.; Kim, J.; Wachter, J. B.; Chae, H. K.; O'Keeffe, M.; Yaghi, O. M. *J. Am. Chem. Soc.* **2001**, *123*, 4368−4369. (b) Chen, L.; Yang, T.; Cui, H.; Cai, T.; Zhang, L.; Su, C.-Y. *J. Mater. Chem. A* **2015**, *3*, 20201.
(16) Dobrzánska, L.; Lloyd, G. O.; Raubenheimer, H. G.; Barbour, L. J. *J. Am. Chem. Soc.* **2006**, *128*, 698−699.
(17) Jacobs, T.; Lloyd, G. O.; Gertenbach, J.-A.; Müller-Nedebock, K. K.; Esterhuysen, C.; Barbour, L. J. *Angew. Chem., Int. Ed.* **2012**, *51*, 4913−4916.
(18) Chen, L.; Reiss, P. S.; Chong, S. Y.; Holden, D.; Jelfs, K. E.; Hasell, T.; Little, M. A.; Kewley, A.; Briggs, M. E.; Stephenson, A.; Thomas, K. M.; Armstrong, J. A.; Bell, J.; Busto, J.; Noel, R.; Liu, J.; Strachan, D. M.; Thallapally, P. K.; Cooper, A. I. *Nat. Mater.* **2014**, *13*, 954−960.

(19) Avellaneda, A.; Valente, P.; Burgun, A.; Evans, J. D.; Markwell-Heys, A. W.; Rankine, D.; Nielsen, D. J.; Hill, M. R.; Sumby, C. J.; Doonan, C. J. *Angew. Chem., Int. Ed.* **2013**, *52*, 3746.
(20) Liu, X.; Warmuth, R. *J. Am. Chem. Soc.* **2006**, *128*, 14120.
(21) O'Reilly, N.; Giri, N.; James, S. L. *Chem. - Eur. J.* **2007**, *13*, 3020.
(22) Rouquerol, J.; Avnir, D.; Fairbridge, C. W.; Everett, D. H.; Haynes, J. H.; Pernicone, N.; Ramday, J. D. F.; Sing, K. S. W.; Unger, K. K. *Pure Appl. Chem.* **1994**, *66*, 1739−1758.
(23) (a) Atwood, J. L.; Davies, J. E. D.; MacNichol, D. D. *Inclusion Compounds*; Academic Press: London, U.K., 1984. (b) Powell, H. M. *J. Chem. Soc.* **1948**, 61−73.
(24) (a) Allison, S. A.; Barrer, R. M. *J. Chem. Soc. A* **1969**, *0*, 1717. (b) Barrer, R. M.; Shanson, V. H. *J. Chem. Soc., Chem. Commun.* **1976**, 333. (c) Su, D.; Wang, X.; Simard, M.; Wuest, J. D. *Supramol. Chem.* **1995**, *6*, 171. (d) Hosseini, M. W. *Acc. Chem. Res.* **2005**, *38*, 313.
(25) Thallapally, P. K.; McGrail, P. B.; Dalgarno, S. J.; Schaef, H. T.; Tian, J.; Atwood, J. L. *Nat. Mater.* **2008**, *7*, 146.
(26) Jones, J. T. A.; Holden, D.; Mitra, T.; Hasell, T.; Adams, D. J.; Jelfs, K. E.; Trewin, A.; Willock, D. J.; Day, G. M.; Bacsa, J.; Steiner, A.; Cooper, A. I. *Angew. Chem., Int. Ed.* **2011**, *50*, 749.
(27) Tian, J.; Thallapally, P. K.; Liu, J.; Exarhos, G. J.; Atwood, J. L. *Chem. Commun.* **2011**, *47*, 701.
(28) Kitaigorodsky, A. I. *Molecular Crystal and Molecules*; Academic Press: New York, 1973.
(29) Atwood, J. L.; Barbour, L. J.; Jerga, A. *Science* **2002**, *296*, 2367−2369.
(30) Barbour, L. J. *Chem. Commun.* **2006**, 1163−1168.
(31) (a) Pinalli, R.; Suman, M.; Dalcanale, E. *Eur. J. Org. Chem.* **2004**, *2004*, 451. (b) Pirondini, L.; Dalcanale, E. *Chem. Soc. Rev.* **2007**, *36*, 695. (c) Pinalli, R.; Dalcanale, E. *Acc. Chem. Res.* **2013**, *46*, 399.
(32) Ma, S.; Sun, D.; Wang, X.-S.; Zhou, H.-C. *Angew. Chem., Int. Ed.* **2007**, *46*, 2458.
(33) Tanaka, D.; Henke, A.; Albrecht, K.; Moeller, M.; Nakagawa, K.; Kitagawa, S.; Groll, J. *Nat. Chem.* **2010**, *2*, 410.
(34) Takasaki, Y.; Takamizawa, S. *J. Am. Chem. Soc.* **2014**, *136*, 6806.
(35) Warmuth, R.; Marvel, M. A. *Chem. - Eur. J.* **2001**, *7*, 1209.
(36) O'Neil, A.; Wilson, C.; Webster, J. M.; Allison, F. J.; Howard, J. A. K.; Poliakoff, M. *Angew. Chem., Int. Ed.* **2002**, *41*, 3796.
(37) Momma, K.; Ikeda, T.; Nishikubo, K.; Takahashi, N.; Honma, C.; Takada, M.; Furukawa, Y.; Nagase, T.; Kudoh, Y. *Nat. Commun.* **2011**, *2*, 196.
(38) Corbin, D. R.; Abrams, L.; Jones, G. A.; Smith, M. L.; Dybowski, C. R.; Hriljac, J. A.; Parise, J. *J. Chem. Soc., Chem. Commun.* **1993**, 1027.
(39) (a) Cram, D. J. *Science* **1983**, *219*, 1177. (b) Moran, J. R.; Karbach, S.; Cram, D. J. *J. Am. Chem. Soc.* **1982**, *104*, 5826. (c) Cram, D. J.; Steward, K. D.; Goldberg, I.; Trueblood, K. N. *J. Am. Chem. Soc.* **1985**, *107*, 2574. (d) Cram, D. J.; Karbach, S.; Kim, H.-E.; Knobler, C. B.; sMaverick, E. F.; Ericson, J. L.; Helgeson, R. C. *J. Am. Chem. Soc.* **1988**, *110*, 2229. (e) Cram, D. J.; Cram, J. M. In *Container Molecules and Their Guests*; Stoddart, J. F., Ed.; The Royal Society of Chemistry: Cambridge, U.K., 1994.
(40) Lara-Ochoa, F.; Garcia, M. M.; Teran, R.; Almaza, R. C.; Espinoza-Perez, G.; Chen, G.; Silaghi-Dumitrescu, I. *Supramol. Chem.* **2000**, *11*, 263.
(41) (a) Takamizawa, S.; Nataka, E.; Akatsuka, T.; Miyake, R.; Kakizaki, Y.; Takeuchi, H.; Maruta, G.; Takeda, S. *J. Am. Chem. Soc.* **2010**, *132*, 3783. (b) Takamizawa, S.; Nakata, E.; Miyake, R. *Dalton Trans.* **2009**, 1752. (c) Takamizawa, S.; Nakata, E.; Akasuka, T.; Kachi-Terajima, C.; Miyake, R. *J. Am. Chem. Soc.* **2008**, *130*, 17882.
(42) (a) Banerjee, D.; et al. *Acc. Chem. Res.* **2015**, *48*, 211−219. (b) Chen, X.; Plonka, A. M.; Banerjee, D.; Krishna, R.; Schaef, H. T.; Ghose, S.; Thallapally, P. K.; Parise, J. B. *J. Am. Chem. Soc.* **2015**, *137*, 7007.
(43) Kane, C. M.; Holman, K. T. Cavitand compositions and methods of use thereof. WO 2013191778A3, Mar 22, 2013.
(44) See Supporting Information for discussion on issues of pore volume and V_{cav}, PF_{cav}, guest occupancy determination by single crystal diffraction and validation by TGA.
(45) Spek, A. T. *Acta Crystallogr.* **2015**, *C71*, 9.
(46) Kawaguchi, T.; Tanaka, K.; Takeuchi, T.; Watanabe, T. *Bull. Chem. Soc. Jpn.* **1973**, *46*, 62.
(47) Atwood, J. L.; Hamada, F.; Robinson, K. R.; Orr, G. W.; Vincent, R. L. *Nature* **1991**, *349*, 683.
(48) Fucke, K.; Anderson, K. M.; Filby, M. H.; Henry, M.; Wright, J.; Mason, S. A.; Gutmann, M. J.; Barbour, L. J.; Oliver, C.; Coleman, A. W.; Atwood, J. L.; Howard, J. A. K.; Steed, J. W. *Chem. - Eur. J.* **2011**, *17*, 10259.
(49) Sheldrick, G. M. *Acta Crystallogr., Sect. A: Found. Crystallogr.* **2008**, *A64*, 112.
(50) Cram, D. J.; Stewart, K. D.; Goldberg, I.; Trueblood, K. N. *J. Am. Chem. Soc.* **1985**, *107*, 2574.
(51) IUPAC-NIST Solubility Database, Version 1.1, NIST Standard Reference Database 106, http://srdata.nist.gov/solubility/index.aspx, accessed 9/2015.
(52) Horike, S.; Shimomura, S.; Kitagawa, S. *Nat. Chem.* **2009**, *1*, 695.
(53) Mason, J. A.; Oktawiec, J.; Taylor, M. K.; Hudson, M. R.; Rodriguez, J.; Bachman, J. E.; Gonzalez, M. I.; Cervellino, A.; Guagliardi, A.; Brown, C. M.; Llewellyn, P. L.; Masciocchi, N.; Long, J. R. *Nature* **2015**, *527*, 357−361.
(54) Hawxwell, S.; Espallargas, G. M.; Bradshaw, D.; Rosseinsky, M. J.; Prior, T. J.; Florence, A. J.; van de Streek, J.; Brammer, L. *Chem. Commun.* **2007**, 1532.
(55) Lien, P.-Y.; You, R.-M.; Hu, W.-P. *J. Phys. Chem. A* **2001**, *105*, 2391−2400.
(56) Demaison, J.; Breidung, J.; Thiel, W.; Papousek, D. *Struct. Chem.* **1999**, *10*, 129.
(57) van Nes, G. J. H.; Vos, A. *Acta Crystallogr., Sect. B: Struct. Crystallogr. Cryst. Chem.* **1977**, *B33*, 1653.
(58) van Nes, G. J. H.; Vos, A. *Acta Crystallogr., Sect. B: Struct. Crystallogr. Cryst. Chem.* **1979**, *B35*, 2593.
(59) Podsiadło, M.; Olejniczak, A.; Katrusiak, A. *CrystEngComm* **2014**, *16*, 8279.
(60) Podsiadło, M.; Bujak, M.; Katrusiak, A. *CrystEngComm* **2012**, *14*, 4496.
(61) Ilczyszyn, M.; Selent, M.; Ilczyszyn, M. M. *J. Phys. Chem. A* **2012**, *116*, 3206.
(62) Khawam, A.; Flanagan, D. R. *J. Phys. Chem. B* **2006**, *110*, 17315.

DOI: 10.1021/jacs.5b11395
J. Am. Chem. Soc. 2016, 138, 4377−4392